

THE ENERGY SPECTRUM OF PRIMARY COSMIC RAY ELECTRONS IN CLUSTERS OF GALAXIES AND INVERSE COMPTON EMISSION

CRAIG L. SARAZIN

Department of Astronomy, University of Virginia,
 P.O. Box 3818, Charlottesville, VA 22903-0818;
 cls7i@virginia.edu

Submitted to the Astrophysical Journal, January 6, 1999

ABSTRACT

Models for the evolution of the integrated energy spectrum of primary cosmic ray electrons in clusters of galaxies have been calculated, including the effects of losses due to inverse Compton (IC), synchrotron, and bremsstrahlung emission, and Coulomb losses to the intracluster medium (ICM). The combined time scale for these losses reaches a maximum of $\sim 3 \times 10^9$ yr for electrons with a Lorentz factor $\gamma \sim 300$. A variety of models for the time evolution of particle injection are considered, including models in which the electrons are all produced at a single epoch in the past, models with continuous particle acceleration, and combinations of these. Analytical solutions are given for a number of limiting cases. Numerical solutions are given for more general cases. Only clusters in which there has been a substantial injection of relativistic electrons since $z \lesssim 1$ will have any significant population of primary cosmic ray electrons at present. For models in which all of the electrons were injected in the past, there is a high energy cutoff γ_{\max} to the present electron distribution. At low energies where Coulomb losses dominate, the electron distribution function $N(\gamma)$ tends to a constant value, independent of γ . On the other hand, if electrons are being accelerated at present, the energy distribution at high and low energies approaches steady state. If the electrons are injected with a power-law distribution, the steady state distribution is one power steeper at high energies and one power flatter at low energies. In models with a large initial population of particles, but also with a significant rate of current particle injection, the electron distributions are a simple combination the behavior of the initial population models and the steady injection models. There is a steep drop in the electron population at γ_{\max} , but higher energy electrons are present at a rate determined by the current rate of particle injection. Increasing the ICM thermal gas density decreases the number of low energy electrons ($\gamma \lesssim 100$). If the magnetic field is greater than generally expected, ($B \gtrsim 3 \mu\text{G}$), synchrotron losses will reduce the number of high energy electrons. A significant population of electrons with $\gamma \sim 300$, associated with the peak in the particle loss time, is a generic feature of the models, as long as there has been significant particle injection since $z \lesssim 1$.

The IC and synchrotron emission from these models was calculated. In models with steady particle injection with a power-law exponent p , the IC spectra relax into a steady-state form. At low energies, the spectrum is a power-law with $\alpha \approx -0.15$, while at high energies $\alpha \approx -1.15$. These two power-laws meet at a knee at $\nu \sim 3 \times 10^{16}$ Hz. In models with no current particle injection, the cutoff in the electron distribution at high energies ($\gamma \geq \gamma_{\max}$) results in a rapid drop in the IC spectrum at high frequencies. In models in which the current rate of particle injection provides a small but significant fraction of the total electron energy, the spectra show an extended hump at low frequencies ($\nu \lesssim 10^{17}$ Hz), with a rapid fall off above $\nu \sim 10^{16}$ Hz. However, they also have an extended hard tail of emission at high frequencies, which has a power-law spectrum with a spectral index of $\alpha \approx -1.15$.

In the models, EUV and soft X-ray emission are nearly ubiquitous. This emission is produced by electrons with $\gamma \sim 300$, which have the longest loss times. The spectra are predicted to drop rapidly in going from the EUV to the X-ray band. The IC emission also extends down the UV, optical, and IR bands, with a fairly flat spectrum ($-0.6 \gtrsim \alpha \gtrsim +0.3$). At hard X-ray energies $\gtrsim 20$ keV, IC emission should become observable against the background of thermal X-ray emission. Such hard X-ray (HXR) emission is due to high energy electrons ($\gamma \sim 10^4$). The same electrons will produce diffuse radio emission (cluster radio halos) via synchrotron emission. Because of the short loss times of these particles, HXR and diffuse radio emission are only expected in clusters which have current (or very recent) particle acceleration. Assuming that the electrons are accelerated in ICM shocks, one would only expect diffuse HXR/radio emission in clusters which are currently undergoing a large merger. The luminosity of HXR emission is primarily determined by the current rate of particle acceleration in the cluster. The spectra in most models with significant HXR or radio emission are approximately power-laws with $\alpha \approx -1.1$. The IC spectrum from the EUV to HXR are not generally fit by a single power-law. Instead, there is a rapid fall-off from EUV to X-ray energies, with a power-law tail extending into the HXR band.

Subject headings: cosmic rays — galaxies: clusters: general — intergalactic medium — radiation mechanisms: nonthermal — ultraviolet: general — X-rays: general

1. INTRODUCTION

Early X-ray observations with the *Uhuru* satellite established that clusters of galaxies were luminous, extended X-ray sources (Cavaliere, Gursky, & Tucker 1971). The X-ray emission is due

to hot ($\sim 10^8$ K), diffuse intracluster gas (see Sarazin [1988] for a review). This intracluster medium (ICM) contains heavy elements with abundances, relative to hydrogen, of about one third of the solar values. The gas is thought to have originated mainly from infall of intergalactic gas, although the heavy ele-

ments probably came from gas ejected by galaxies. The gas is believed to have been shock-heated during infall into the cluster, during subcluster mergers, and as a portion of it was ejected by galaxies.

It is useful to compare the intracluster medium with the interstellar medium which fills the volumes of space between stars in our Galaxy. The interstellar medium in our Galaxy contains a mixture of at least three different types of matter: thermal gases of various densities and temperatures; solid dust grains; and relativistic materials, including magnetic fields and cosmic ray particles. To what extent would one expect to find similar materials in the intracluster medium? It may be difficult for dust grains and cooler thermal gas phases to survive in the hot ICM. However, there is no obvious reason why clusters should not contain magnetic fields and relativistic particles.

In fact, there are a number of reasons to think that cosmic ray particles might be particularly abundant within the intracluster medium. First, clusters of galaxies should be very effective traps for cosmic ray ions and electrons. Under reasonable assumptions for the diffusion coefficient, particles with energies of less than $\lesssim 10^6$ GeV have diffusion times which are longer than the Hubble time (Berezinsky, Blasi, & Ptuskin 1997; Colafrancesco & Blasi 1998). Second, the lifetimes of cosmic ray particles, even the electrons which are responsible for most of the radiative signatures of relativistic particles, can be quite long. The radiation fields (optical/IR and X-ray) and magnetic fields ($B \lesssim 1 \mu\text{G}$) in the ICM are low enough that high energy electrons mainly lose energy by inverse Compton (IC) scattering of Cosmic Microwave Background (CMB) photons (Sarazin & Lieu 1998). Lower energy electrons can lose energy by Coulomb interactions with the plasma; however, at the very low densities ($n_e \lesssim 10^{-3} \text{ cm}^{-3}$) in the bulk of the ICM, this is only important for electrons with $\gamma \lesssim 200$ (Sarazin & Lieu 1998). (Here, γ is the Lorentz factor for the electrons, so that their total energy is $\gamma m_e c^2$.) For electrons with $\gamma \gtrsim 200$, the lifetime is set by IC losses and is

$$t_{IC} = \frac{(\gamma - 1)m_e c^2}{\frac{4}{3}\sigma_T c \gamma^2 U_{CMB}} \approx 7.7 \times 10^9 \left(\frac{\gamma}{300}\right)^{-1} \text{ yr}. \quad (1)$$

The lifetimes of ions are set by interactions; for protons, this gives $t_{ion} \gtrsim 10^{11} (n_e / 10^{-3} \text{ cm}^{-3})^{-1} \text{ yr}$. Thus, clusters of galaxies can retain low energy electrons ($\gamma \sim 300$) and nearly all cosmic ray ions for a significant fraction of a Hubble time.

Cluster of galaxies are likely to have substantial sources of cosmic rays. Clusters often contain powerful radio galaxies, which may produce and distribute cosmic rays throughout the cluster, in addition to possible contributions from the cluster galaxies. However, the primary reason why the cosmic ray populations in clusters might be large is connected with the high temperature of the intracluster gas. This indicates that all of the intracluster medium (typically, $10^{14} M_\odot$ of gas) has passed through strong shocks with shock velocities of $\sim 1000 \text{ km/s}$ during its history. In our own Galaxy, whenever diffuse gas undergoes a strong shock at velocities of this order, a portion of the shock energy goes into the acceleration of relativistic particles (Blandford & Ostriker 1978; Bell 1978a,b; Blandford & Eichler 1987; Jones & Ellison 1991). Thus, it seems likely that relatively efficient particle acceleration also occurs in clusters of galaxies.

Direct evidence for the presence of an extensive population of relativistic particles and magnetic fields in the ICM comes from the observation of diffuse synchrotron radio halos in clus-

ters (e.g., Wilson 1970; Hanisch 1982; Giovannini et al. 1993; Deiss et al. 1997). More recently, extreme ultraviolet (EUV) and very soft X-ray emission has been detected from a number of clusters (Lieu et al. 1996a,b; Mittaz, Lieu, & Lockman 1998). Although the origin and even the existence of this radiation remain controversial, one hypothesis is that it is inverse Compton (IC) emission by relativistic electrons (Hwang 1997; Enßlin & Biermann 1998; Sarazin & Lieu 1998). Finally, there are a number of reports of detections of hard X-ray emission from clusters of galaxies with *BeppoSAX*, which might be due to IC emission from higher energy electrons (Fusco-Femiano et al. 1998; Kaastra, Bleeker, & Mewe 1998), although this interpretation is still uncertain (Henriksen 1998; Goldoni et al. 1998). The EUV emission would require electrons with $\gamma \sim 300$, while the hard X-ray emission would require $\gamma \sim 10^4$.

The *BeppoSAX* detection of hard X-ray emission from Coma implies that the average magnetic field over large volumes of the cluster is $0.16 \mu\text{G}$. Faraday rotation measurements towards Coma and other clusters suggest that the magnetic field in the core of the cluster is stronger, perhaps around $1 \mu\text{G}$ (Kim et al. 1990; Kim, Kronberg, & Tribble 1991; Kronberg 1994). In our models, we will use $0.3 \mu\text{G}$ as a typical value for the intracluster magnetic field on large scales.

The energy spectra of relativistic particles in many astrophysical environments are often modeled as power-laws. The energy spectrum of cosmic ray electrons in clusters of galaxies have been represented as power-laws in most investigations (e.g., Hwang 1997; Enßlin & Biermann 1998). This should be a reasonable approximation at energies where all of the particles are relativistic and where there are no other physical scales affecting the energy. However, there are a number of reasons why the populations of relativistic electrons in clusters of galaxies might not be well-represented by power-laws. First, at the low energies of interest for the EUV emission ($\gamma \sim 300$, or $E \sim 150 \text{ MeV}$, where E is the particle kinetic energy), the electrons are relativistic, but the ions are not. Second, at the energies of interest for the EUV emission ($\gamma \sim 300$), the life times of the electrons are close to the Hubble time (eq. 1). At much higher or lower energies, the electron life times are much shorter. Thus, losses affect different parts of the electron energy spectrum in different ways. Finally, at low energies $\gamma \lesssim 200$, the electrons mainly lose energy to the plasma due to Coulomb losses. At higher energies $\gamma \gtrsim 200$, the most important losses are due to IC or synchrotron emission. These different loss mechanisms have different energy dependences, and this breaks any simple scaling in the particle losses.

In this paper, illustrative models will be calculated for the energy spectrum of primary, relativistic electrons. Recently, models in which the relativistic electrons are secondaries produced by interactions of cosmic ray ions have been given by Colafrancesco & Blasi (1998). In this paper, we will concentrate on the total energy spectrum of all the relativistic electrons in the cluster, under the assumption that they remain trapped in the cluster (Berezinsky et al. 1997; Colafrancesco & Blasi 1998). In a subsequent paper, we will discuss the spatial distribution of the cosmic ray particles.

2. EVOLUTION OF THE ELECTRON SPECTRUM

2.1. Evolution Equation

The evolution of the cosmic ray electron population in clusters is given by the diffusion-loss equation (Ginzburg & Sy-

rovatskii 1964):

$$\frac{dn(E)}{dt} = -n(E)\nabla \cdot \mathbf{v} + \nabla \cdot [D(E)\nabla n(E)] + \frac{\partial}{\partial E} [b(E)n(E)] + q(E), \quad (2)$$

where $n(E)dE$ is the number density of electrons with kinetic energies in the range E to $E+dE$, \mathbf{v} is the velocity of the ICM, d/dt is the Lagrangian time derivative, $D(E)$ is the diffusion coefficient, and $q(E)dE$ gives the rate of production of new cosmic ray particles per unit volume with energies in the range E to $E+dE$. The losses by the particles are given by $b(E) \equiv -(dE/dt)$, where the derivative gives the rate of change in the energy of a single particle with an energy of E . This formulation of the losses assumes that they are continuous; this is a reasonable approximation for the Coulomb and inverse Compton losses which are most important for electrons in clusters, but is not completely correct for bremsstrahlung losses. Equation (2) ignores the acceleration of the electrons (which we will treat separately and include in q) and their generation as secondaries through the interaction of other particles.

Here, we consider models for the total cosmic ray electron spectrum of clusters, without considering the spatial distribution of the particles. Let $N(E)dE$ be the total number of electrons in the cluster with kinetic energies in the range E to $E+dE$. I will also assume that cosmic ray electrons and ions are trapped within clusters, and cannot escape. Models for cosmic ray diffusion within clusters do indeed suggest that they should be trapped (Berezinsky et al. 1997; Colafrancesco & Blasi 1998). Then, integrating equation (2) over the volume of the cluster leads to an equation for the time evolution of the total electron spectrum,

$$\frac{\partial N(E)}{\partial t} = \frac{\partial}{\partial E} [b(E)N(E)] + Q(E), \quad (3)$$

where $Q(E)dE$ gives the total rate of production of new cosmic ray electrons in the energy range E to $E+dE$. I have replaced $b(E)$ by its value averaged over all the particles in the cluster. The first two terms on the right hand side of equation (2) are converted by Green's formula into fluxes at the outer surface of the cluster, which are zero since we assume that the cluster retains all of the particles.

I will use the Lorentz factor γ of the electrons as the independent variable rather than the kinetic energy $E = (\gamma - 1)m_e c^2$, where m_e is the electron mass. With the definitions $N(\gamma)d\gamma = N(E)dE$, $Q(\gamma)d\gamma = Q(E)dE$, and $b(\gamma) = b(E)/m_e c^2$, the expression for the energy loss by an individual particle becomes

$$\frac{d\gamma}{dt} = -b(\gamma, t), \quad (4)$$

and the equation for the evolution of the electron populations is

$$\frac{\partial N(\gamma)}{\partial t} = \frac{\partial}{\partial \gamma} [b(\gamma)N(\gamma)] + Q(\gamma). \quad (5)$$

2.2. Loss Rates

The loss function $b(\gamma)$ for inverse Compton scattering of the Cosmic Microwave Background (CMB) is given by

$$b_{IC}(\gamma) = \frac{4}{3} \frac{\sigma_T}{m_e c} \gamma^2 U_{CMB} = 1.37 \times 10^{-20} \gamma^2 (1+z)^4 \text{ s}^{-1}, \quad (6)$$

where σ_T is the Thomson cross-section, and U_{CMB} is the energy density in the CMB at the cluster, and z is the redshift of

the cluster. The numerical value follows from the present CMB temperature of $T_{CMB} = 2.73$ K and the redshift evolution of the CMB energy density.

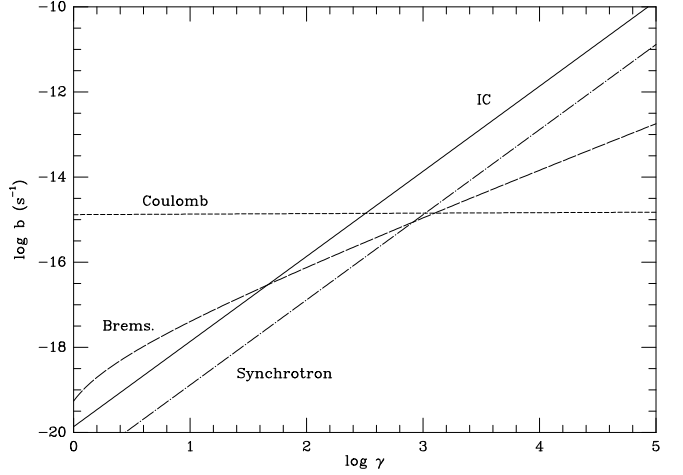


FIG. 1.— The values of the losses function $b(\gamma)$ for inverse Compton (IC) emission, Coulomb losses, synchrotron losses, and bremsstrahlung losses as a function of γ . The values assume $n_e = 10^{-3} \text{ cm}^{-3}$, $B = 1 \mu\text{G}$, and $z = 0$.

The expression for the loss rate due to synchrotron radiation is the same as that in equation (6) if one substitutes the energy density in the magnetic field $U_B = B^2/(8\pi)$ for the CMB energy density:

$$b_{syn}(\gamma) = \frac{4}{3} \frac{\sigma_T}{m_e c} \gamma^2 U_B = 1.30 \times 10^{-21} \gamma^2 \left(\frac{B}{1 \mu\text{G}} \right)^2 \text{ s}^{-1}, \quad (7)$$

where B is the magnetic field in the ICM. Both equations (6) and (7) assume $\gamma \gg 1$. Obviously, the loss rates for IC and for synchrotron losses vary in the same manner with γ . The intra-cluster field is estimated to have a values of roughly $B \sim 1 \mu\text{G}$ (e.g., Rephaeli, Gruber, & Rothschild 1987; Kim et al. 1990). As long as the field is not much stronger than this, IC losses will dominate over synchrotron losses, with

$$\frac{b_{syn}}{b_{IC}} = \frac{U_B}{U_{CMB}} \approx 0.095 (1+z)^4 \left(\frac{B}{1 \mu\text{G}} \right)^2. \quad (8)$$

The relativistic electrons will also lose energy by interactions with the thermal plasma. The Coulomb losses due to collisions with thermal ions and electrons give a loss rate which is approximately (e.g., Rephaeli 1979)

$$b_{Coul}(\gamma) \approx 1.2 \times 10^{-12} n_e \left[1.0 + \frac{\ln(\gamma/n_e)}{75} \right] \text{ s}^{-1}, \quad (9)$$

where n_e is the thermal electron density in the cluster. The same collisions between cosmic ray electrons and thermal particles also produce radiation through bremsstrahlung. For the completely unscreened limit which is appropriate to a low density plasma, the loss rate due to bremsstrahlung is given approximately by (e.g., Blumenthal & Gould 1970)

$$b_{brem}(\gamma) \approx 1.51 \times 10^{-16} n_e \gamma [\ln(\gamma) + 0.36] \text{ s}^{-1}, \quad (10)$$

The values of these loss functions as a function of γ are given in Figure 1 for an intracluster medium (ICM) electron density

of $n_e = 1.0 \times 10^{-3} \text{ cm}^{-3}$ and a typical ICM magnetic field of $B = 1 \mu\text{G}$. It is clear from this Figure and the expressions for the loss functions that IC losses are dominant at large energies, $\gamma \gtrsim 200$, while Coulomb losses dominate for sufficiently small $\gamma \lesssim 200$ or for higher densities. Bremsstrahlung losses are unlikely to be dominant unless the density is higher than is typical in the bulk of the ICM (outside of cooling flow regions). Similarly, synchrotron losses are unlikely to be dominant unless the magnetic field is much stronger than $1 \mu\text{G}$.

2.3. Electron Lifetimes

One can define an instantaneous time scale for particle losses by

$$t_{\text{loss}} \equiv \frac{\gamma}{b(\gamma)}. \quad (11)$$

Values for this loss time scale at the present time ($z = 0$) are shown in Figure 2. The solid curve gives values assuming an average electron density of $n_e = 10^{-3} \text{ cm}^{-3}$ and a magnetic field of $B = 1 \mu\text{G}$. For values of the magnetic field this small or lower, synchrotron losses are not very significant, and t_{loss} is nearly independent of B . The short dashed curve shows the effect of increasing the magnetic field to $B = 5 \mu\text{G}$; the losses at high energies are increased, and the loss time scales shortened. The dash-dot curve shows the loss time scale if the electron density is lowered to $n_e = 10^{-4} \text{ cm}^{-3}$. This reduces the losses at low energies, and increases the loss times there.

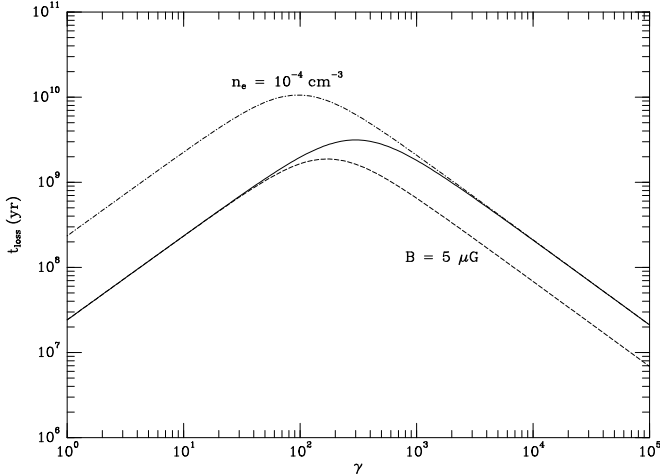


FIG. 2.— The solid curve gives the instantaneous loss time scale t_{loss} (eqn. 11) as a function of γ for electrons in a cluster with an electron density of $n_e = 10^{-3} \text{ cm}^{-3}$ and a magnetic field of $B = 1 \mu\text{G}$. The short-dash curve is for $B = 5 \mu\text{G}$, while the dash-dot curve is for $n_e = 10^{-4} \text{ cm}^{-3}$.

The characteristic features of t_{loss} for parameters relevant to clusters are that it has a maximum at $\gamma \sim 100-500$, and that the maximum loss time is quite long, unless either the magnetic field or electron density are larger than typical values for most of the volume of a cluster. The maximum loss times are $\sim 3-10 \text{ Gyr}$, which is comparable to the likely ages of clusters. Thus, particles can accumulate with $\gamma \sim 300$ for long periods in clusters. In § 3.1 below, we will show that although electrons at $\gamma \sim 300$ can accumulate for a significant fraction of the Hubble time, the increase in the energy density of the CMB implies that the accumulation period is restricted to $z \lesssim 1$.

3. ANALYTIC SOLUTIONS

A number of simple analytic solutions for the evolution of the cosmic ray population (eq. 5) are possible. I will consider two simple classes of solutions: solutions with an initial population of particles $N(\gamma, t_i)$ at some initial time t_i or redshift z_i but no subsequent injection of additional particles [$Q(\gamma) = 0$]; and solutions with no initial population [$N(\gamma, t_i) = 0$] but with continual injection of particles at a rate $Q(\gamma, t)$. Since equation (5) is linear in $N(\gamma, t)$, any solution can be written as a superposition of these two solutions.

3.1. Initial Injection Only

3.1.1. General Solution

First, consider a case where there is no continual source of new particles ($Q = 0$). Then, the population simply evolves due to the loss of energy by individual particles. At this point, assume that the loss function $b(\gamma, t)$ is an arbitrary function of γ and time t . Given an initial value for the energy of a particle γ_i at time t_i , equation (4) can be integrated to give the value of γ at a later time t . Alternatively, equation (4) can be integrated backward in time to give the initial energy $\gamma_i(\gamma, t, t_i)$ at t_i corresponding to a particle with energy γ at a later time t . If there is no subsequent injection of particles, then the number of particles is conserved if one follows their energies. This implies that

$$\int_{\gamma_i}^{\infty} N(\gamma', t) d\gamma' = \int_{\gamma_i}^{\infty} N(\gamma', t_i) d\gamma'. \quad (12)$$

The differential population density is then given by

$$N(\gamma, t) = N(\gamma_i, t_i) \left. \frac{\partial \gamma_i}{\partial \gamma} \right|_t. \quad (13)$$

3.1.2. Constant Loss Function

For periods of time which are short compared to the Hubble time, the total loss function $b(\gamma)$ may be approximately independent of time. If a particle starts (at time $t = t_i$) with a Lorentz factor γ_i , after a time $t - t_i$ its energy will have been reduced to γ , where

$$\int_{\gamma}^{\gamma_i} \frac{d\gamma'}{b(\gamma')} = (t - t_i). \quad (14)$$

Applying this energy loss to the entire electron population, one finds that the electron spectrum evolves as

$$N(\gamma, t) = N[\gamma_i(\gamma, t), t_i] \frac{b[\gamma_i(\gamma, t)]}{b(\gamma)}, \quad (15)$$

where $\gamma_i(\gamma, t)$ is given implicitly by equation (14).

3.1.3. Solution at High Energies: Non-Cosmological

IC losses dominate at high energies. If we consider the evolution over time scales which are shorter than the age of the Universe, so that the redshift z is approximately constant, then the loss function at high energies can be written as

$$b(\gamma) \approx b_1 \gamma^2 \quad \gamma \gg 10^2, \quad (16)$$

where the numerical constant b_1 is given in equation (6). The single particle loss equation (14) gives

$$\gamma_i = \frac{\gamma}{1 - \frac{\gamma}{\gamma_{\text{max}}}}. \quad (17)$$

After the passage of a time $\Delta t \equiv (t - t_i)$, all of the electrons with energies above γ_{\max} will have been removed, where

$$\gamma_{\max} = \frac{1}{b_1 \Delta t}. \quad (18)$$

Thus, the resulting electron distribution is related to the initial distribution by

$$N(\gamma, t) = \begin{cases} \frac{N[\gamma/(1-\gamma/\gamma_{\max}), t_i]}{(1-\gamma/\gamma_{\max})^2} & \gamma < \gamma_{\max} \\ 0 & \gamma \geq \gamma_{\max} \end{cases} \quad (19)$$

If the initial particle distribution was a power-law with $N(\gamma_i, t_i) = N_1 \gamma_i^{-p_0}$, then the resulting final distribution is

$$N(\gamma, t) = \begin{cases} N_1 \gamma^{-p_0} (1 - \gamma/\gamma_{\max})^{p_0-2} & \gamma < \gamma_{\max} \\ 0 & \gamma \geq \gamma_{\max} \end{cases} \quad (20)$$

These equations also apply if there is a significant magnetic field in the cluster, since the energy losses from synchrotron emission have the same dependence on γ as those for IC scattering. The value of b_1 would be increased to include synchrotron losses according to equations (6) and (7).

3.1.4. Solution at High Energies: Cosmological

These expressions do not apply to the evolution of the electron energy spectrum over cosmological time scales because of the variation in the energy density of the CMB with redshift z . As a result, the loss rate due to IC emission varies with electron energy and redshift as (eq. 6)

$$b_{IC}(\gamma, z) = b_1 \gamma^2 (1+z)^4. \quad (21)$$

The equation for the evolution of the energy of a single particle subject to IC losses is then

$$\frac{d\gamma}{\gamma^2} = -b_1 (1+z)^4 dt. \quad (22)$$

The age of the Universe t and redshift z are related implicitly by the equation of cosmic dynamics (e.g., Weinberg 1972),

$$t = \frac{1}{H_0} \int_0^{(1+z)^{-1}} \left(1 - 2q_0 + \frac{2q_0}{x} \right)^{-1/2} dx, \quad (23)$$

here H_0 is the Hubble constant and q_0 is the deceleration parameter at the present time.

After some algebra, equation (22) can be integrated to yield the current γ for an electron which had an initial energy of γ_i at a redshift z_i :

$$\frac{1}{\gamma} - \frac{1}{\gamma_i} = \frac{b_1}{H_0} f(q_0, z_i), \quad (24)$$

where the function $f(q_0, z)$ is defined by

$$f(q_0, z) \equiv \frac{1}{15q_0^3} \left[\sqrt{1+2q_0z} (2 - 10q_0 + 15q_0^2 - 2q_0z) + 10q_0^2z + 3q_0^2z^2 - 2 + 10q_0 - 15q_0^2 \right]. \quad (25)$$

For $q_0 = 0$, the limit of equation (25) is

$$f(0, z) = z \left(1 + z + \frac{z^2}{3} \right). \quad (26)$$

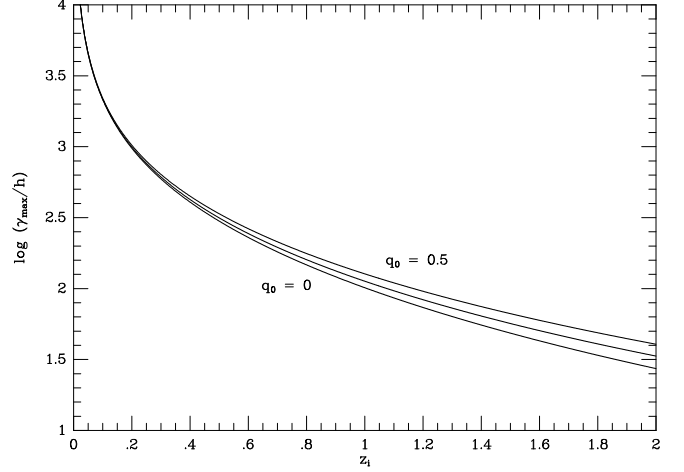


FIG. 3.— The present values of the maximum remaining electron Lorentz factor γ_{\max} is shown as a function of the redshift z_i at which the electrons were last injected in the cluster. Only IC losses are included. Curves are shown for three cosmological models with values of the cosmic deceleration parameter of $q_0 = 0, 0.2$, and 0.5 . The values of γ_{\max} are scaled to the value of the present Hubble constant, with $h \equiv (H_0/100 \text{ km s}^{-1} \text{ Mpc}^{-1})$.

The cosmological expression for the maximum remaining energy of electrons subject to IC losses is then

$$\gamma_{\max} = \frac{H_0}{b_1} \frac{1}{f(q_0, z_i)}. \quad (27)$$

Figure 3 shows values of the maximum Lorentz factor as a function of the redshift z_i for cosmological models with values of $q_0 = 0, 0.2$, and 0.5 . The values of γ_{\max} are scaled by $h \equiv (H_0/100 \text{ km s}^{-1} \text{ Mpc}^{-1})$.

3.1.5. Solution at High Energies with Synchrotron Losses

If the ICM magnetic field is much stronger than is currently believed, synchrotron losses might be important for high energy electrons. Then, the expressions for the cosmological evolution of an initial electron population at high energies would be modified in a way which would depend on the temporal variation of the magnetic field. If the magnetic field were constant, then the losses at high energies could be written as

$$b(\gamma, z) \approx \gamma^2 [b_1^{IC} (1+z)^4 + b_1^{syn}], \quad (28)$$

where the values of b_1^{IC} and b_1^{syn} can be found from equations (6) and (7). Then the evolution of the energy of a single particle at high energies is given by

$$\frac{1}{\gamma} - \frac{1}{\gamma_i} = \frac{1}{H_0} \{ b_1^{IC} f(q_0, z_i) + b_1^{syn} [g(q_0, 0) - g(q_0, z_i)] \}, \quad (29)$$

where $g(q_0, z)$ is the integral on the right side of equation (23). This function is most easily given in the standard parametric form (e.g., Weinberg 1972)

$$g(q_0, z) = \begin{cases} (1+z)^{-1} & q_0 = 0 \\ \frac{q_0 [\sinh(\theta) - \theta]}{(1-2q_0)^{3/2}} & \cosh(\theta) = 1 + \frac{1-2q_0}{q_0} \frac{1}{1+z} \quad 0 < q_0 < 1/2 \\ \frac{2}{3} (1+z)^{-3/2} & q_0 = 1/2 \\ \frac{q_0 [\theta - \sin(\theta)]}{(2q_0-1)^{3/2}} & \cos(\theta) = 1 - \frac{2q_0-1}{q_0} \frac{1}{1+z} \quad 1/2 < q_0 \end{cases} \quad (30)$$

Then, the upper cutoff in the electron energy distribution is given by

$$\gamma_{\max} = \frac{H_0}{b_1^C f(q_0, z_i) + b_1^{\text{syn}} [g(q_0, 0) - g(q_0, z_i)]}. \quad (31)$$

The resulting particle distributions are still given by equations (19) or (20), with the correct value for γ_{\max} . If one wants to calculate the particle distribution at an intermediate redshift z ($0 < z < z_i$) rather than at present ($z = 0$), then one substitutes $[f(q_0, z_i) - f(q_0, z)]$ for $f(q_0, z_i)$ and $g(q_0, z)$ for $g(q_0, 0)$ in equations (24), (27), (29), and (31).

3.1.6. Solution at Low Energies

At low electron energies, the dominant losses will be due to Coulomb collisions. Coulomb losses have the property that they vary only rather slowly (logarithmically) with γ (eq. 9). Here, this slow variation is ignored, and the Coulomb losses are written as $b(\gamma, t) = b_{\text{Coul}} \approx b_C$, where b_C is a constant given by the value in equation (9) for some appropriate value of γ , say $\gamma \sim 10^2$. Then, equation (14) for the change in γ for a single particle gives

$$\gamma = \gamma_i - \gamma_{\text{low}}, \quad (32)$$

where the characteristic value γ_{low} is defined by

$$\gamma_{\text{low}} \equiv b_C \Delta t. \quad (33)$$

The equation for the evolution of the electron population (eq. 15) reduces to

$$N(\gamma, t) \approx N[\gamma + \gamma_{\text{low}}, t_i]. \quad (34)$$

For a short time $\Delta t \ll \gamma/b_C$, the population is nearly the initial one. However, the Coulomb losses at low electron energies will tend to be rapid. Thus, after a time $\Delta t \gg \gamma/b_C$, the population will approach

$$N(\gamma, t) \approx N[\gamma_{\text{low}}, t_i]. \quad (35)$$

That is, the population at low energies will vary with time, but will be nearly independent of γ ,

$$N(\gamma) \approx N_{\text{low}}(t) = \text{constant}. \quad (36)$$

3.2. Steady Injection Only

As an alternative to the case where there is an initial population of particles but no continual source, we consider the case where there is continuous injection of particles at a constant rate $Q(\gamma)$, but where there is no initial electron population.

3.2.1. Steady-State Solutions

At energies where the time scale for losses by particles t_{loss} is much shorter than the age of the cluster, the population will tend towards a steady-state distribution. From Figure 2, this is likely to occur at high energies ($\gamma \gtrsim \gamma_{\max}$) due to rapid IC and synchrotron losses. It may also occur at low energies ($\gamma \lesssim \gamma_{\text{low}}$) due to rapid Coulomb losses. If $t_{\text{loss}} \equiv [\gamma/b(\gamma)] \ll \Delta t$, then it is likely that $\partial N(\gamma, t)/\partial t \ll \partial [b(\gamma, t)N(\gamma, t)]/\partial \gamma$. In steady-state ($\partial/\partial t = 0$), the equation for the evolution of the electron population (eq. 5) becomes

$$\frac{d}{d\gamma} [b(\gamma)N(\gamma)] = -Q(\gamma). \quad (37)$$

If there is no flux of particles from infinite energies and if $\lim_{\gamma \rightarrow \infty} b(\gamma)N(\gamma) \rightarrow 0$, then the steady-state solution is given by

$$N(\gamma) = \frac{1}{b(\gamma)} \int_{\gamma}^{\infty} Q(\gamma') d\gamma'. \quad (38)$$

It is useful to consider a source which is a power-law function of the electron energy, with

$$Q(\gamma) = Q_1 \gamma^{-p}, \quad (39)$$

with $p > 1$. Then, at high energies where IC and synchrotron losses dominate and we can write the loss function as $b(\gamma) \approx b_1 \gamma^2$, the resulting electron distribution is

$$N(\gamma) = \frac{Q_1}{b_1(p-1)} \gamma^{-(p+1)}; \quad (40)$$

that is, the resulting electron distribution is one power steeper than the source. At low energies where Coulomb losses dominate, the losses depend only logarithmically on the electron energy. If we ignore this slow dependence and take $b(\gamma) \approx b_C$ (a constant), then the resulting steady-state distribution is

$$N(\gamma) = \frac{Q_1}{b_C(p-1)} \gamma^{-(p-1)}; \quad (41)$$

that is, the resulting electron distribution is one power flatter than the source. These classical results were derived first by Ginzburg (e.g., Ginzburg & Syrovatskii 1964).

3.2.2. Self-Similar Solutions

For simple approximations for the loss function and simple expressions for the rate of injection $Q(\gamma)$, one can often find self-similar solutions which connect the steady-state population with non-steady populations which are time dependent. In these solutions, the overall normalization of the electron population varies with time, but the shape of the energy spectrum remains the same if γ is scaled by some characteristic value.

At high energies where IC and synchrotron losses dominate, one can approximate the loss function by equation (16), at least at low redshifts. The characteristic value of γ at high energies is γ_{\max} (eq. 18). Then, if the particle injection follows a power-law distribution (eq. 39), the self-similar solution for the electron population is given by

$$N(\gamma, t) = \frac{Q_1}{b_1(p-1)} \gamma^{-(p+1)} \begin{cases} 1 - (1 - \gamma/\gamma_{\max})^{p-1} & \gamma < \gamma_{\max} \\ 1 & \gamma \geq \gamma_{\max} \end{cases}. \quad (42)$$

At low energies where Coulomb losses dominate, the loss rate is nearly independent of γ , $b(\gamma) \approx b_C$. Then, the characteristic value of the γ is γ_{low} (eq. 33). For a power-law spectrum of injected particles (eq. 39), the self-similar solution for the electron population is given by

$$N(\gamma, t) = \frac{Q_1}{b_C(p-1)} \gamma^{-(p-1)} \left[1 - (1 + \gamma_{\text{low}}/\gamma)^{-(p-1)} \right]. \quad (43)$$

At energies where losses are not important ($\gamma \ll \gamma_{\max}$ in equation [42] and $\gamma \gg \gamma_{\text{low}}$ in equation [43]), the two self-similar solutions are identical, $N(\gamma, t) \approx Q(\gamma)t$. That is, the population is just the sum of the injected particles at that energy, as expected if losses have not affected the energies of the particles. If $\gamma_{\text{low}} \ll \gamma_{\max}$, then the two solutions can simply be

joined in this central region. With some algebra, one finds that this solution can be written as

$$N(\gamma, t) \approx \frac{Q_1 \gamma^{-p} t}{p-1} \left(\frac{\gamma_{low}}{\gamma} + \frac{\gamma}{\gamma_{max}} \right)^{-1} \times \left\{ 2 - \left[\frac{1}{2} \left(1 - \frac{\gamma}{\gamma_{max}} + \left| 1 - \frac{\gamma}{\gamma_{max}} \right| \right) \right]^{p-1} - \left(1 + \frac{\gamma_{low}}{\gamma} \right)^{-(p-1)} \right\}. \quad (44)$$

This solution applies for all γ as long as $\gamma_{low} \ll \gamma_{max}$.

4. SOURCE FUNCTION FOR ELECTRONS

4.1. Injected Electron Spectrum

Models will be calculated which include an initial population of relativistic electrons and/or continuous injection of relativistic electrons during the history of the cluster. Although the models don't depend on the details of the processes which accelerate relativistic electrons in clusters, the basic assumption is that these particles result from shock or turbulent acceleration. The shocks and turbulence might be associated with the hydrodynamical evolution of the ICM; for example, the initial population might be due to an accretion shock during the formation of the cluster, and semi-continuous particle injection might result from subcluster mergers. Alternatively, the shocks might be due to the expansion of radio sources within the ICM.

The condition for the shocks due to the hydrodynamics of the intracluster medium are similar to condition in Galactic supernova remnants (SNRs), except that the length scales are much larger and the densities are smaller. Over a significant range of relativistic energies, there is considerable theoretical and observational evidence that such shock acceleration produces particles with a power-law distribution (e.g., Blandford & Eichler 1987; Jones & Ellison 1991). Thus, we will consider models in which the initial electron spectrum at $t = t_i$ is a single power-law,

$$N(\gamma, t_i) = N_1 \gamma^{-p_0}, \quad (45)$$

and/or the continuous source of injected electrons is a power-law,

$$Q(\gamma, t) = Q_1(t) \gamma^{-p}. \quad (46)$$

For typical strong shock compressions, one expects values of $p = p_0 \approx 2.3$ (e.g., Blandford & Eichler 1987; Jones & Ellison 1991).

One complication in applying the standard results on shock acceleration to the ICM is that we need to determine the population of relatively low energy cosmic ray electrons ($\gamma \sim 300$) in order to calculate their EUV emission. Such particles have kinetic energies (~ 150 MeV) for which electrons are relativistic, but protons and other ions are not. There are a number of simple arguments which suggest that the energy spectrum of superthermal but subrelativistic particles is a flatter power-law than for fully relativistic particles (Bell 1978b). The suggestion is that the *momentum* spectrum of particles accelerated in shocks is the same power-law for both relativistic and nonrelativistic particles and for both ions and electrons. That is, $Q(P)dP \propto P^{-p}dP$, where P is the particle momentum and $Q(P)dP$ gives number of particles accelerated with momenta between P and $P+dP$ per unit time. For highly relativistic particles $E = Pc$, but for non-relativistic particles the kinetic energy $E = P^2/2m$, where m is their mass. Under the same assumptions which result in a shock acceleration energy spectrum of highly relativistic particles with $Q(E) \propto E^{-p}$, the energy spectrum for superthermal

but subrelativistic particles is $Q(E) \propto E^{-(p+1)/2}$. For a typical relativistic injection spectrum with $p \approx 2.3$, the subrelativistic spectrum would have a lower exponent $p_l \approx 1.65$. At energies $E \sim 100$ MeV, this would only affect the shock acceleration spectrum of ions. Bell (1978b) suggests that would result in the total number of accelerated electrons and ions (at energies above $m_e c^2$) being nearly equal, while the number of ions with $E \gg m_p c^2$ would be larger than that of electrons at the same energies.

However, it is also possible the the spectrum of shock accelerated electrons would also be affected. Thus, we will also consider models in which the initial electron spectrum at $t = t_i$ is a broken power-law,

$$N(\gamma, t_i) = N_1 \times \begin{cases} \gamma^{-p_l} & \gamma < \gamma_{br} \\ \gamma_{br}^{-p_l} \left(\frac{\gamma}{\gamma_{br}} \right)^{-p_0} & \gamma \geq \gamma_{br} \end{cases} \quad (47)$$

and/or the continuous source of injected electrons is a broken power-law, with

$$Q(\gamma, t) = Q_1(t) \begin{cases} \gamma^{-p_l} & \gamma < \gamma_{br} \\ \gamma_{br}^{-p_l} \left(\frac{\gamma}{\gamma_{br}} \right)^{-p} & \gamma \geq \gamma_{br} \end{cases} \quad (48)$$

4.2. Normalization of the Electron Population

Equation 5 for the evolution of the population is linear in $N(\gamma)$, so the solution can be rescaled by increasing or decreasing $N(\gamma, t)$, the initial value $N(\gamma, t_i)$, and the electron injection rate $Q(\gamma, t)$ by any constant factor. Thus, the normalization of the solution is arbitrary. I have chosen an arbitrary normalization; however, it is at least somewhat consistent with energetic and stability arguments concerning the ICM medium, with the observed EUV fluxes of clusters, and with the observed properties of shock acceleration in SNRs in our Galaxy. If the observed EUV radiation from clusters results from IC scattering of CMB photons by cosmic ray electrons, the observed EUV luminosities imply that clusters contain cosmic ray electrons with $\gamma \gtrsim 300$ which have a total energy of the order of $E_{CR,e} \sim 10^{62}$ ergs. It is also unlikely that the cosmic ray energy significantly exceeds the thermal energy of the ICM, since this would likely result in the ICM being expelled from the clusters. Rich clusters contain approximately $10^{14} M_\odot$ of hot gas at a typical temperature of 7×10^7 K, which implies that the thermal energy content of the gas is approximately $E_{gas} \sim 4 \times 10^{63}$ ergs. Thus, if the cosmic ray electrons had a total kinetic energy of $E_{CR,e} \sim 10^{62}$ ergs, this would represent approximately 3% of the thermal energy content of the ICM. Even when one includes the contribution from cosmic ray ions, this ratio is likely to remain of order unity or smaller. Finally, we note that the radio observations of Galactic SNR imply that shock acceleration produces cosmic ray electrons which contain at least a few per cent of the shock energy (e.g., Blandford & Eichler 1987). Since essentially all of the thermal energy content of the ICM is the result of shock heating (§ 1 above), these shocks should also have accelerated relativistic electrons containing at least a few per cent of the thermal energy content of the intracluster medium.

I have chosen to normalize the electron spectra so that the total amount of kinetic energy injected in electrons with $\gamma \geq 300$ is $E_{CR,e}^{tot} = 10^{63}$ ergs. In the models which seem most likely to represent real, present day clusters, this leads to present day electron populations with $E_{CR,e} \sim 10^{62}$ ergs.

4.3. Self-Similar Cluster Accretion Shock

In most of the models with continual injection of particles, we assume for simplicity that the injection rate is constant over the time that it acts, $\partial Q(\gamma, t)/\partial t = 0$. As an alternative, we consider a simple model for the cosmological evolution of $Q(\gamma, t)$. Bertschinger (1985) has given a simple, self-similar solution for the secondary accretion of intracluster gas (with or without associated dark matter) onto a previously collapsed cluster core. This solution applies only in an Einstein-de Sitter Universe, with $\Omega = 1$ and $\Lambda = 0$. In the Bertschinger solution, the accretion shock radius expands with time as $r_s \propto t^{8/9}$, and the preshock density varies with the average cosmological density $\rho \propto t^{-2}$. The shock velocity obviously varies as $v_s \propto r_s/t \propto t^{-1/9}$. In this solution, the preshock gas is cold and the accretion shock is always very strong. Thus, rate of shock energy input varies as $\dot{E}_{shock} = (1/2)\rho v_s^3 4\pi r_s^2 \propto t^{-5/9}$.

If we assume that a given fraction of the shock energy goes into accelerating the relativistic electrons, then it is useful to give the rate of shock energy input at any time in terms of the total shock energy over the life time of the cluster. Integration of the shock energy equation leads to the following expression for the accretion shock energy input in the Bertschinger self-similar solution:

$$\frac{\dot{E}_{shock}(z)}{E_{shock}} = \frac{4}{9} \frac{1}{t_o} \frac{(1+z)^{5/6}}{1 - (1+z_i)^{-2/3}}, \quad (49)$$

where t_o is the present age of the Universe, z is the redshift at the time when the shock energy is being evaluated, and z_i is the redshift at which the cluster formed.

5. NUMERICAL MODELS

5.1. Techniques

A number of numerical models for the integrated energy spectra of cosmic ray electrons in clusters of galaxies have been calculated. For models with an initial electron population at redshift z_i but no subsequent particle injection, the population was calculated by following the energy losses of individual particles. That is, equation (4) was integrated backward in time to determine the initial Lorentz factor γ_i corresponding to the present day γ for a large number of particles with energies in the range $1 < \gamma \leq 10^5$. The loss equation was integrated using the Bulirsch-Stoer technique with adaptive step-size control (e.g., Press et al. 1986). The equation of cosmic dynamics (eq. 23) was used to relate redshift and co-moving time. All of the loss processes discussed in § 2.2 were included. Then, the present day electron spectrum was determined from particle conservation through equation (13).

For models with continual injection but no initial population, the equation for the evolution of the electron energy spectrum (eq. 5) was integrated with a finite-difference technique on a fixed grid of energies covering the range $1 < \gamma \leq 10^5$. I found that the energy spectrum at very high energies was well-represented by the self-similar solution (eq. 42). I assumed this solution applied at high energies beyond the upper end of the grid, and it was used to determine the flux of particles into the grid from higher energies. The time step was regulated so that the flux of particles into each grid cell from higher energies was a small fraction ($< 1\%$) of the population of that cell, and so that the redshift step was also very small.

Because the equation for the evolution of the electron population is linear (eq. 5), models with both an initial populations and

subsequent particle injection were created by the superposition of solutions with only an initial population and only subsequent injection.

Unless otherwise noted, the average thermal electron density in the ICM was taken to be $n_e = 0.001 \text{ cm}^{-3}$, the Hubble constant was $H_0 = 65 \text{ km s}^{-1} \text{ Mpc}^{-1}$, and the magnetic field was $B = 0.3 \text{ } \mu\text{G}$. In all of the models, the deceleration parameter was $q_0 = 0.5$.

In all of the models, there is a population of particles with $\gamma \approx 1$, which represent initially relativistic electrons which have returned to the thermal population through energy losses. Since the number of cosmic ray electrons is small compared to the number of thermal electrons, this population is probably not important.

Some of the assumed properties of the numerical models are summarized in Table 1. The models start at a redshift of z_i . In models with continual particle injection, this starts at z_s . The value of the Hubble constant in the models is given in column 4. The average thermal electron density n_e and magnetic field B are given in columns 5 and 6. A “Y” in the columns labeled “Initial” or “Cont.” indicates whether the model includes an initial population of relativistic electron at z_i and/or whether there is continual particle injection since z_s . The values of p_0 , p , γ_{br} , and p_l indicate the form of the power-law or broken power-law injection spectrum, according to equations (45)–(48). If no value is given for γ_{br} , the injection spectrum is a single power-law (eqs. 45–46). For models with both an initial population and continual particle injection, the value of F_{inj} is the fraction of the total particle energy which is contributed by the continual particle injection. The last column gives a comment on the model.

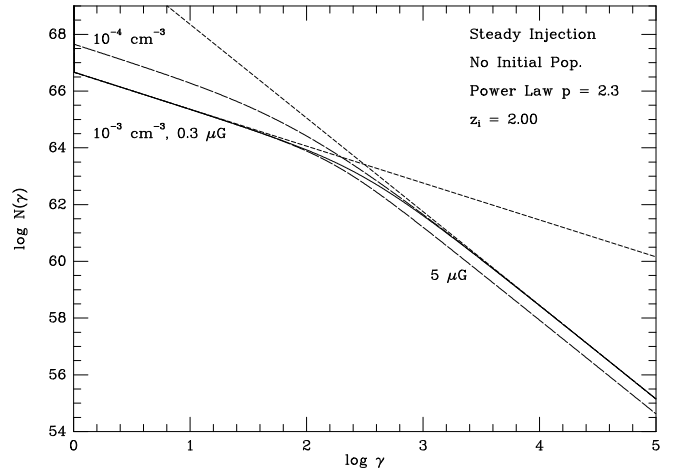


FIG. 4.— The relativistic electron population in a cluster in which particles have been injected at a constant rate since $z_i = 2$. The injected particles had a power-law distribution with $p = 2.3$. The solid curve (Model 1) is the distribution in a cluster with an average thermal electron density of $n_e = 10^{-3} \text{ cm}^{-3}$. The two short-dashed lines are power-law distributions with $p' = 1.3$ and 3.3 , which match the resulting particle distributions at low and high energy, respectively. The two long-dashed curves are similar to Model 1, but have a decreased electron density of $n_e = 10^{-4} \text{ cm}^{-3}$ (Model 7) or an increased magnetic field of $B = 5 \text{ } \mu\text{G}$ (Model 8).

5.2. Solutions

Some of the results for the numerical models for the electron population in clusters are given in Table 2. For each model, the second column gives the total number of relativistic elec-

TABLE 1
NUMERICAL MODELS FOR THE ELECTRON SPECTRUM

Model	z_i	z_s	H_0 (km s ⁻¹ Mpc ⁻¹)	n_e (cm ⁻³)	B (μG)	Initial Pop.	p_0	Cont. Inj.	p	γ_{br}	p_l	F_{inj} (%)	Comment
1	2.00	2.00	65	0.001	0.3	N		Y	2.3			100	Steady injection
2	1.00	1.00	65	0.001	0.3	N		Y	2.3			100	Steady injection
3	0.50	0.50	65	0.001	0.3	N		Y	2.3			100	Steady injection
4	0.30	0.30	65	0.001	0.3	N		Y	2.3			100	Steady injection
5	0.10	0.10	65	0.001	0.3	N		Y	2.3			100	Steady injection
6	0.01	0.01	65	0.001	0.3	N		Y	2.3			100	Steady injection
7	2.00	2.00	65	0.0001	0.3	N		Y	2.3			100	Model 1, but lower density
8	2.00	2.00	65	0.000	5.0	N		Y	2.3			100	Model 1, but stronger magnetic field
9	0.01		65	0.001	0.3	Y	2.3	N				0	Initial pop. only
10	0.10		65	0.001	0.3	Y	2.3	N				0	Initial pop. only
11	0.30		65	0.001	0.3	Y	2.3	N				0	Initial pop. only
12	0.50		65	0.001	0.3	Y	2.3	N				0	Initial pop. only
13	1.00		65	0.001	0.3	Y	2.3	N				0	Initial pop. only
14	0.30		65	0.0001	0.3	Y	2.3	N				0	Model 11, but lower density
15	0.30		100	0.001	0.3	Y	2.3	N				0	Model 11, but larger H_0
16	0.30		65	0.001	0.0	Y	2.3	N				0	Model 11, but no magnetic field
17	0.30		65	0.001	1.0	Y	2.3	N				0	Model 11, but stronger magnetic field
18	0.30		65	0.001	3.0	Y	2.3	N				0	Model 11, but stronger magnetic field
19	0.30		65	0.001	5.0	Y	2.3	N				0	Model 11, but stronger magnetic field
20	2.00	2.00	65	0.001	0.3	N		Y	2.3			100	Bertschinger model
21	2.00	2.00	65	0.001	0.3	N		Y	2.3	2000	1.3	100	Broken power-law injection
22	0.30		65	0.001	0.3	Y	2.3	N		2000	1.3	0	Broken power-law initial pop.
23	0.05	0.05	65	0.001	0.3	N		Y	2.3			100	Steady injection
24	0.30	0.05	65	0.001	0.3	Y	2.3	Y	2.3			50	Both init. pop. & current inj.
25	0.30	0.05	65	0.001	0.3	Y	2.3	Y	2.3			25	Both init. pop. & current inj.
26	0.30	0.05	65	0.001	0.3	Y	2.3	Y	2.3			10	Both init. pop. & current inj.
27	0.30	0.05	65	0.001	0.3	Y	2.3	Y	2.3			1	Both init. pop. & current inj.
28	0.30	0.05	65	0.001	0.3	Y	2.3	Y	2.3			0.1	Both init. pop. & current inj.

trons N_{tot} at present (at $z = 0$). Columns 3 and 4 give the kinetic energy in relativistic electrons at present ($z = 0$), either for all of the electrons ($\gamma > 1$) or only for those with $\gamma > 300$. The fifth column gives the energy-averaged mean value of γ , defined here as

$$\langle \gamma \rangle \equiv \frac{\int N(\gamma) \gamma^2 d\gamma}{\int N(\gamma) \gamma d\gamma}. \quad (50)$$

Sarazin & Lieu (1998) show that this quantity is useful for estimating the emission properties of these electrons. For models without particle injection at the present time (§ 5.2.2), the last column gives the upper cut off to the electron distribution, γ_{max} .

5.2.1. Steady Particle Injection

I first considered models in which relativistic electrons are injected into the ICM at a constant rate over the history of the cluster, and there was no initial population of electrons. Figure 4 shows the result of steady injection since an initial redshift of $z_i = 2$; the solid curve is for Model 1 in Table 1. For this large redshift, the age of the cluster exceeds the loss time of the electrons for all values of γ (Figure 2). This is particularly true when one includes the increase in the energy density of the CMB with redshift. For example, Figure 3 shows that IC losses will remove all of the particles produced at $z \sim 1$ down to low values of γ where Coulomb losses dominate and the lifetime is short. Thus, one expects that the particle distribution will approach steady state, with the rate of injection balancing the rate of loss at most energies. The injected electrons had a

simple power-law distribution (equation 46) with $p = 2.3$. Figure 4 shows that the resulting electron population is essentially a broken power-law. The dashed lines show power-law distributions with indices of $p' = 1.3$ and 3.3 . At lower energies where Coulomb losses dominate ($\gamma \lesssim 100$), the distribution is very nearly a power-law with $p' = 1.3$. This is one power flatter than the injected population, as expected from the steady-state result of equation (41). At high energies where IC and synchrotron losses dominate ($\gamma \gtrsim 1000$), the distribution is nearly a power-law with $p' = 3.3$. This is one power steeper than the injected population, as expected from the steady-state result of equation (40).

The approach to steady-state in models with constant injection is shown in Figure 5, which gives the present day populations in models with initial redshifts of $z_i = 0.01, 0.1, 0.3, 0.5, 1$, and 2 (top to bottom). (These are Models 1–6 in Table 1.) All of the models have an average electron density of $n_e = 10^{-3}$ cm⁻³, and a magnetic field of $B = 0.3$ μG. The particles are injected with a power-law spectrum with $p = 2.3$. The older models ($z_i = 0.5, 1$, and 2) have achieved steady-state, since the loss times of electrons of all energies are less than the age of the cluster. The younger cluster models show departures from steady-state. For these models, the energy spectra of electrons can be divided into three regions. At very high energies ($\gamma \gtrsim \gamma_{max}$), the IC losses are sufficiently rapid that the loss time scale (eqn. 11) is shorter than the age, and the populations approach steady-state, and the population is a power-law which is one power steeper than the injected spectrum. Similarly, at

low energies the loss time scale is also generally shorter than the age (Figure 2). The population also approaches steady-state below some lower value of $\gamma \lesssim \gamma_{\text{low}}$, and population is a power-law which is one power flatter than the injection spectrum. At intermediate energies $\gamma_{\text{low}} \ll \gamma \ll \gamma_{\text{max}}$, the loss time scale is longer than the age, and the population is given by the accumulation of the injection rate. Thus, it has the same spectrum as the injection spectrum. For younger injection models where $\gamma_{\text{low}} \ll \gamma_{\text{max}}$, the resulting electron population is given quite accurately by the self-similar solution (equation 44).

TABLE 2
RESULTS FOR THE ELECTRON ENERGY SPECTRUM

Model	N_{tot} (10^{66})	$E_{\text{CR},e}$		$\langle \gamma \rangle$	γ_{max}
		$\gamma > 1$ (10^{61} ergs)	$\gamma > 300$		
1	11.98	28.39	9.48	544.6	
2	14.96	35.46	11.85	544.6	
3	21.16	50.15	16.81	546.2	
4	29.12	67.32	23.50	564.2	
5	65.38	119.23	42.59	675.7	
6	377.34	264.52	71.55	1159.4	
7	95.67	91.58	11.50	204.7	
8	11.73	21.10	4.29	302.0	
9	118.87	198.19	62.98	761.9	15107
10	7.67	56.76	23.17	334.0	1379
11	1.95	13.38	0.70	153.6	338
12	0.67	2.17	0.00	60.6	110
13	0.00	0.00	0.00	3.1	83
14	44.38	88.65	4.17	93.2	405
15	3.93	28.99	7.67	209.9	582
16	1.95	13.43	0.74	154.4	340
17	1.93	12.82	0.31	147.0	320
18	1.76	9.01	0.00	104.7	211
19	1.44	4.66	0.00	61.6	114
20	8.51	21.01	6.93	527.5	
21	0.54	11.12	8.13	1513.9	
22	0.61	7.57	0.93	212.0	333
23	113.10	159.80	53.50	787.0	
24	57.52	86.59	27.10	740.1	
25	29.74	49.98	13.90	664.4	
26	13.06	28.02	5.98	521.8	
27	3.06	14.84	1.23	224.6	
28	2.06	13.52	0.75	161.5	

Figure 4 also shows the effect of changing the gas density or magnetic field in the models. The two long-dash curves are the same as Model 1, but with the electron density decreased to $n_e = 10^{-4} \text{ cm}^{-3}$ (Model 7) or the magnetic field increased to $B = 5 \mu\text{G}$ (Model 8). Increasing or decreasing the gas density mainly increases or decreases the rate of Coulomb losses at low energies, and this decreases or increases the electron population at low energies. Reducing n_e also decreases the electron energy or value of γ at which the transition between the two power-law slopes occurs in steady-state. Similarly, increasing magnetic field enhances the rate of synchrotron losses at high energies. This reduces the population of at high energies, but the effect is only important if the field exceeds about $3 \mu\text{G}$.

5.2.2. Initial Population with No Later Particle Injection

Next, models were calculated with an initial electron population at a redshift z_i , but with no subsequent injection of particles. Figure 6 shows the result for models with differing values

of the initial redshift z_i . The initial particle population was a single power-law with $p_0 = 2.3$ (eqn. 45). At high energies, the electron population is reduced and the shape of the spectrum steepened by IC and synchrotron losses. There is an upper cut-off to the electron distribution (eqns. 19–20) for values of γ beyond a maximum values γ_{max} , given approximately by equation (27), or equation (18) for low redshifts. The cutoff energies in the numerical models are in reasonable agreement with these analytic approximations as long as $\gamma_{\text{max}} \gtrsim 300$. The value of γ_{max} decreases as the age of the electron populations (or, equivalently, the initial redshift z_i) increases.

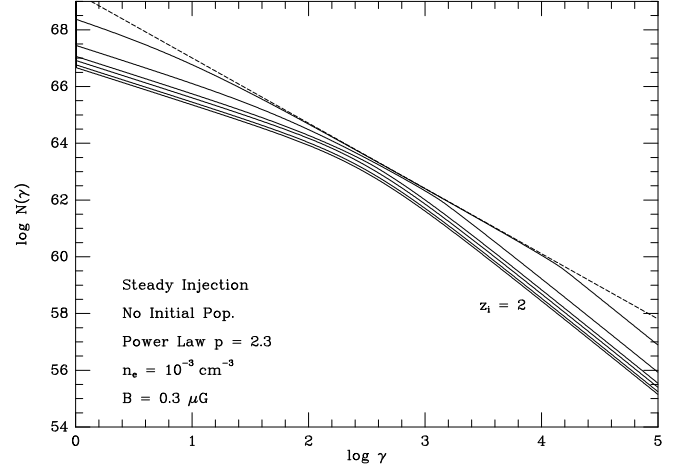


FIG. 5.— The present day relativistic electron populations in a series of models with steady particle injection but no initial population of particles. The solid curves show models for clusters which started at redshifts of $z_i = 2, 1, 0.5, 0.3, 0.1$, and 0.01 (bottom to top). These are Models 1–6 in Table 1. In all of the models, the particles are injected at a constant rate with a power-law distribution with $p = 2.3$. The short-dashed curve gives the total power-law spectrum of all of the injected particle over the cluster lifetime.

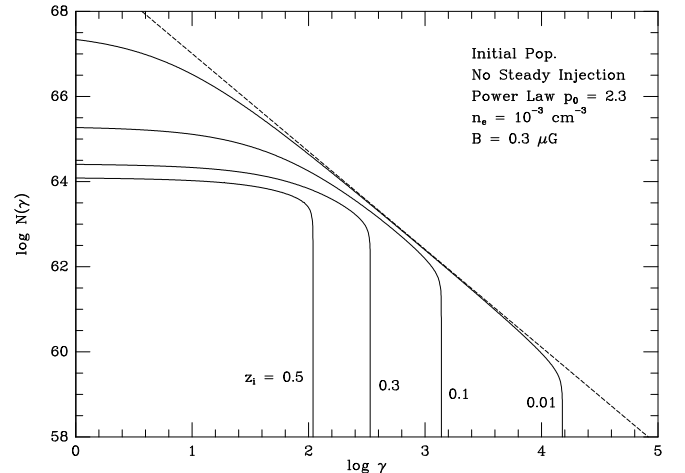


FIG. 6.— The relativistic electron population in models with an initial population of particles generated at a redshift z_i , but no subsequent injection. The initial population, which is shown as a dashed line, had a power-law distribution with $p_0 = 2.3$. The solid curve show the resulting present population for values of the initial redshift of $z_i = 0.01, 0.1, 0.3$, and 0.5 .

In order to have any significant population of primary electrons with $\gamma \gtrsim 10^2$ at the present time, Figures 3 and 6 show that there must have been a substantial injection of particles into clusters at moderately low redshifts, $z \lesssim 1$.

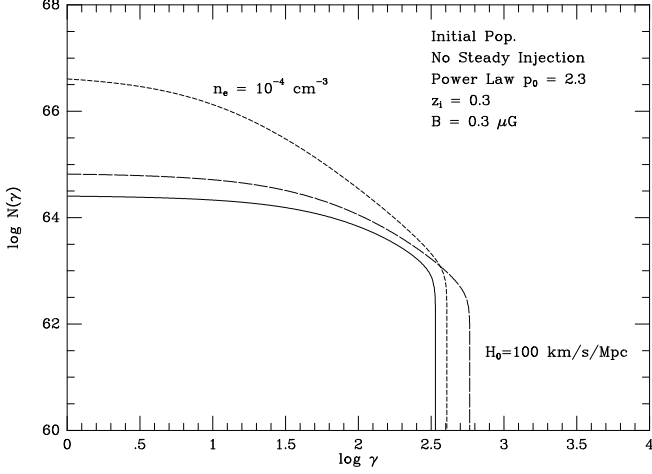


FIG. 7.— The effect on the electron population of changing several of the parameters. The solid curve is Model 11 for an initial population of particles generated at a redshift $z_i = 0.3$, but no subsequent injection. The short-dashed curve (Model 14) shows the result of reducing the average electron density from 10^{-3} to 10^{-4} cm^{-3} . The long-dashed curve (Model 15) shows the result of increasing the Hubble constant from 65 to $100 \text{ km s}^{-1} \text{ Mpc}^{-1}$.

At low energies ($\gamma \lesssim \gamma_{\text{low}}$), the electron population is reduced and the shape of the distribution flattened by Coulomb losses to the thermal plasma. As discussed in § 3.1.6, the slow variation of the Coulomb loss function with γ results in a flat energy spectrum at low energies (eqn. 36). All of the older cluster models in Figure 6 show this behavior. In the younger models ($z_i \lesssim 0.3$), there is an extended region $\gamma_{\text{low}} \lesssim \gamma \lesssim \gamma_{\text{max}}$ where the initial population is preserved. In the older models ($z_i \gtrsim 0.3$), the flat energy spectrum at low energies and steep cut-off at high energies nearly meet, and the energy spectra have a “top hat” form.

Figure 7 shows the effect of varying two of the basic parameters of the models. The solid curve is Model 11, with an average electron density of $n_e = 10^{-3} \text{ cm}^{-3}$ and a Hubble constant of $H_0 = 65 \text{ km s}^{-1} \text{ Mpc}^{-1}$. In all of these models, the electron population was injected into the cluster at $z_i = 0.3$. The short-dashed curve (Model 14) is a model with all of the same parameters, but with a lower value for the electron density of $n_e = 10^{-4} \text{ cm}^{-3}$. Reducing the electron density lowers the rate of Coulomb losses, which dominate at low energies. As a result, increasing or decreasing the electron density decreases or increases the population of low energy electrons.

Changing the value of the Hubble constant changes the age of the cluster for a fixed value of z_i and q_0 . The long-dashed curve in Figure 7 shows Model 15, which has all of the same parameter, except the Hubble constant is increased to $H_0 = 100 \text{ km s}^{-1} \text{ Mpc}^{-1}$. Increasing the Hubble constant shortens the age, and reduces the effect of losses. Thus, the electron population is larger at all energies, and the cutoff value of γ_{max} is increased. Lowering the Hubble constant has the opposite effect.

I also constructed models with a variety of average values for the intracluster magnetic field, which can affect the electron population through synchrotron losses. Figure 8 shows Models 16, 11, and 17–19, with magnetic fields of $B = 0, 0.3, 1.0, 3.0$, and $5.0 \mu\text{G}$. All of the other parameters of Models 16–19 are identical to Model 11. Because synchrotron losses have the same variation with γ as IC losses, they affect the electron population in a very similar way. Unless the ICM magnetic field

exceeds $1 \mu\text{G}$, synchrotron losses do not have a very significant effect. For larger values of B , the number of high energy electrons and the value of γ_{max} are reduced as B is increased. The values of γ_{max} are in good agreement with those predicted by equation (31). However, to produce an appreciable effect, the magnetic field is required to be considerably larger than expected in clusters (Kim et al. 1990, 1991; Kronberg 1994; Fusco-Femiano et al. 1998).

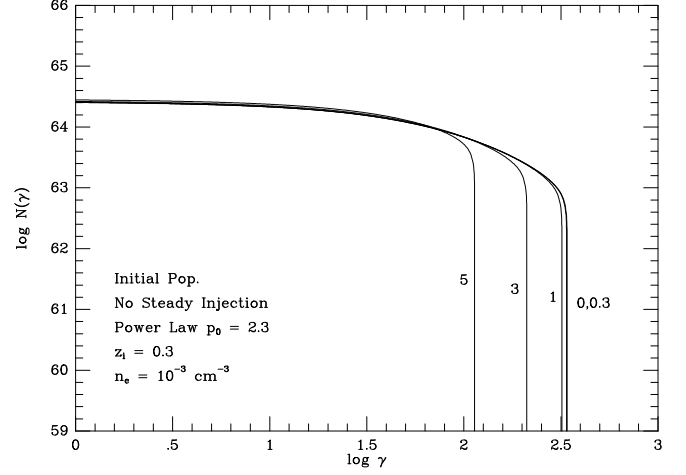


FIG. 8.— Models for relativistic electrons with a variety of intracluster magnetic field strengths (Models 11, 16–19). The curves show the populations for magnetic fields of 0, 0.3, 1, 3, and $5 \mu\text{G}$. The curves for no magnetic field and $0.3 \mu\text{G}$ are nearly indistinguishable.

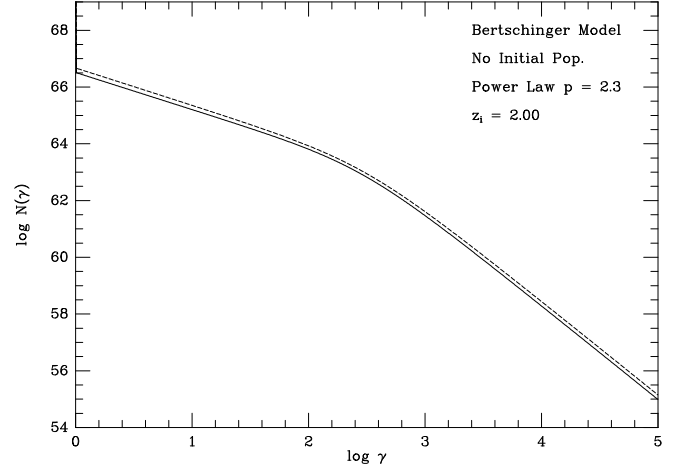


FIG. 9.— The solid curve is the relativistic electron population in a model based on the Bertschinger (1985) self-similar solution for secondary infall in a cluster (eq. [49], Model 20). For comparison, the dashed curve is the steady injection model with the same properties (Model 1).

5.2.3. Self-Similar Cluster Accretion Shock

I also calculated a model in which particles were injected with a rate proportional by the rate of deposition of shock energy (eq. 49) in the self-similar secondary infall model of Bertschinger (1985). In Figure 9, this model (Model 20) is compared to the steady injection model (Model 1) in which the rate of injection of particles is a constant. The two models give very similar results. The small differences between the self-similar secondary infall model and the steady injection model are mainly due to differences in the normalization

(§ 4.2). The models are normalized based on the total input of relativistic electrons, and the Bertschinger model and the steady model have different variations in the rate of injection with time or redshift (eq. 49). If the present day rate of injection is the same, the maximum difference between the Bertschinger model and the steady injection model is only about 10%, and occurs near the knee in the particle spectrum (at $\gamma \approx 160$ in Figure 9). The very near agreement of the Bertschinger model and the steady injection model reflects the fact that both models have nearly reached steady-state, and the current electron spectrum is mainly determined by the present rate of injection, rather than the past rate over cosmological time scales.

5.2.4. Models with Broken Power Law Particle Injection

In § 4.1, we noted that the spectrum of cosmic ray protons produced by shock acceleration is expected to flatten somewhat at kinetic energies $E \lesssim 1$ GeV, where the protons become nonrelativistic. In most models, it is expected that the electron spectrum will remain nearly a power-law to much lower energies. Here, we consider that possibility that the spectrum of electrons also flattens below 1 GeV. I adapt the simple two power-law form of equations 47) and (48). In Figure 10, the resulting electron populations in models with broken power-law models for the initial population or for the injection spectrum. For models with steady injection (Model 21), the broken spectrum produces a low energy electron spectrum which is a flatter power-law by the same amount that the injection spectrum if flattened at low energies. For models with initial broken power-law spectra, the population is very flat at low energies, and has the same high energy cut-off as the model with a single power-law. However, the broken power-law models have a peak at energies just below γ_{\max} if $\gamma_{br} > \gamma_{\max}$.

5.2.5. Models with Both an Initial Population and Steady Injection

Finally, we consider models in which there is an initial population in the cluster at z_i , and in which there also is current injection of new particles. I assume that this current injection has occurred at a constant rate since redshift z_s . These two components might represent particle populations which were produced by shocks associated with the formation of the cluster at z_i and by a current merger event, which started at z_s . Because the equation for the evolution of the electron population is linear (eq. 5), these models are just a linear combination of the models discussed in §§ 5.2.1 and 5.2.2. An illustrative set of such models are shown in Figure 11. I assumed $z_i = 0.3$, $z_s = 0.05$, $n_e = 10^{-3} \text{ cm}^{-3}$, and $B = 0.3 \mu\text{G}$ in these models. Both the initial population and current injection are given by a single power-law spectrum with $p = p_0 = 2.3$. The different models are characterized by differing values of F_{inj} , which is the fraction of the particle energy which has been injected by the current steady injection process, as opposed to the initial population. Models are shown with values of $F_{inj} = 100\%$, 50%, 25%, 10%, 1%, 0.1%, and 0%. (Models 23–28 and 11).

For models with intermediate values of the energy fraction due to the ongoing injection, the energy spectrum at low energies is flatter than the $p' = 1.3$ power-law due to steady state injection, but steeper than the flat distribution expected for the initial population. There is a rapid drop-off in the electron population at γ_{\max} . Above γ_{\max} , the electrons are only due to current injection. Of course, in a real cluster it is unlikely that the initial population would have been produced at a single redshift. Thus, the fall off at γ_{\max} is likely to be more gradual, and there

might be a more continuous transition to the current injection population above γ_{\max} . However, these models should give a general sense of the electron energy spectra to be expected in real clusters.

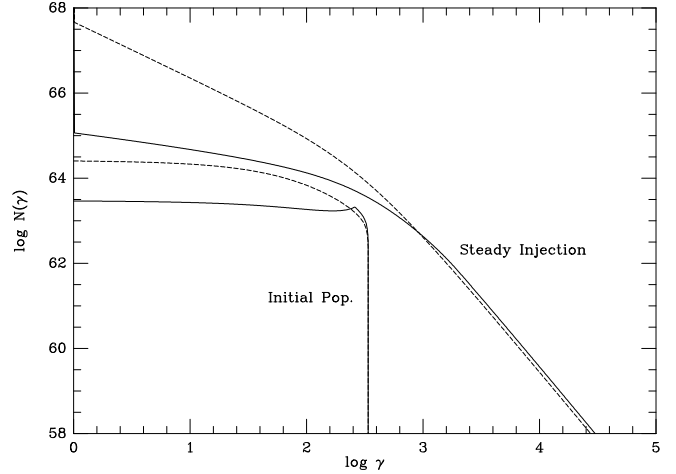


FIG. 10.— Models with broken power-law injection (eq. 48) or initial spectra (eq. 47) are compared to models with simple power-laws. The lower curves compare a model with an initial population (at $z_i = 0.3$) which is a broken power-law (solid curve, Model 22) with an otherwise identical model with a single power-law (dashed curve, Model 11). In these models, there is no subsequent particle injection. The upper curves compare models with no initial population but a steady rate of particle injection since $z_i = 2$. The solid curve has a broken power-law injection spectrum (Model 21), while the dashed curve is for a single power-law (Model 1). For clarity of presentation, the steady injection curves were displaced upwards by one order of magnitude.

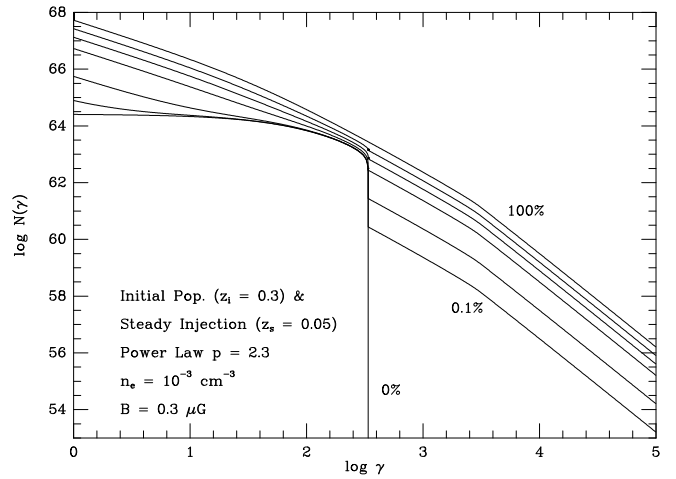


FIG. 11.— The electron energy spectra in models with both an initial electron population starting at $z_i = 0.3$ and continual injection of new particles since $z_s = 0.05$. All of the models have a single power-law spectrum for particle injection with $p = p_0 = 2.3$, an electron density of $n_e = 10^{-3} \text{ cm}^{-3}$, and a magnetic field of $B = 0.3 \mu\text{G}$. The values of the fraction of particle energy due to current injection are (top to bottom) $F_{inj} = 100\%$, 50%, 25%, 10%, 1%, 0.1%, and 0%.

6. INVERSE COMPTON EMISSION

I also calculated the emission produced by the relativistic electron populations due to the inverse Compton scattering of CMB photons. Let $L_\nu d\nu$ be the luminosity of IC emission at frequencies from ν to $\nu + d\nu$. Then, the spectrum of IC emis-

sion is related to the electron spectrum $N(\gamma)$ by

$$L_\nu = 12\pi\sigma_T \int_1^\infty N(\gamma) d\gamma \int_0^1 J\left(\frac{\nu}{4\gamma^2 x}\right) \mathcal{F}(x) dx, \quad (51)$$

where

$$\mathcal{F}(x) \equiv 1 + x + 2x \ln x - 2x^2. \quad (52)$$

Here, $J(\nu)$ is the mean intensity at a frequency ν of the radiation field being scattered. For the CMB, this is just the black body function

$$J(\nu) = B_\nu(T_{\text{CMB}}) = \frac{2h\nu^3}{c^2} \frac{1}{\exp(h\nu/kT_{\text{CMB}}) - 1}. \quad (53)$$

Figure 12 shows the IC spectra of a series of models with a steady rate of particle injection, but no initial electron population. These are the same models (Models 1–6) whose electron populations were shown in Figure 5. The models shown have had steady injection starting at redshifts $z_i = 2, 1, 0.5, 0.3, 0.1$, and 0.01 (bottom to top) and continuing to the present. The dashed line is the spectrum produced by a model in which the electron population is just that injected into the cluster; since this involves no evolution, this model is equivalent to $z_i = 0$. For this model with no evolution, the spectrum is a power-law $L_\nu \propto \nu^\alpha$, where $\alpha = -(p-1)/2$. This gives $\alpha = -0.65$ for the injection spectrum of $p = 2.3$. At frequencies above 10^{17} Hz, the spectrum quickly steepens with time due to IC losses, and becomes a half power steeper, $\alpha \approx -(p/2) \approx -1.15$. At low frequencies, the spectrum flattens more gradually due to Coulomb losses, approaching a spectrum which is a half power flatter, $\alpha \approx -(p-2)/2 \approx -0.15$. If the steady injection has occurred since a redshift of $z_i \gtrsim 0.2$, the spectrum is near that of a steady-state electron population, with these two power-laws meeting at a knee at $\nu \sim 3 \times 10^{16}$ Hz.

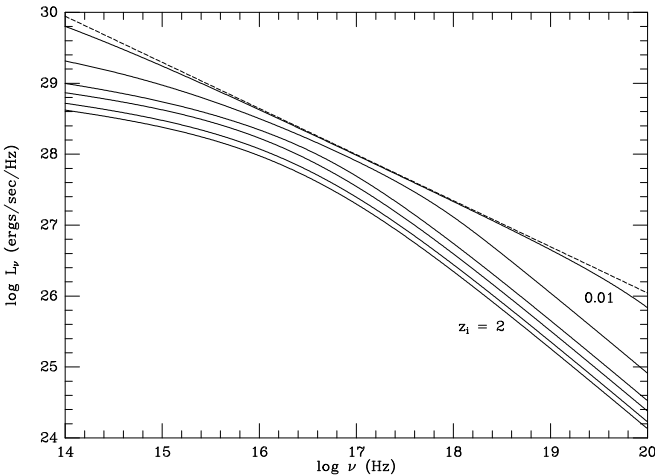


FIG. 12.— The IC emission spectra for cluster models with steady particle injection but no initial population of particles. The notation is similar to that in Figure 5. The solid curves show spectra for clusters which started at redshifts of $z_i = 2, 1, 0.5, 0.3, 0.1$, and 0.01 (bottom to top). These are Models 1–6 in Table 1. The dashed curve gives the spectrum for $z_i = 0$ (i.e., no evolution of the electron population due to losses).

The IC spectra of models with an initial electron population but no subsequent acceleration are shown in Figure 13. This Figure gives the spectra for the same models shown in Figure 6, in which the initial population of electrons occurs at redshifts

of $z_i = 0, 0.01, 0.1, 0.3$, and 0.5 . The electron energy distributions of these models have a cut off at high energies, γ_{max} , which results from rapid IC and synchrotron losses by high energy electrons (see eqs. 18, 27, 31, and Figure 3). As a result, the IC spectra have a very rapid fall off at high energies. If the initial electron spectrum is a power-law with an index of p_0 (eq. 45), and if γ_{max} is large enough that the energy losses are dominated by IC and synchrotron losses, then the electron energy spectrum at a later time is given by equation (20). For this electron spectrum, the IC radiation spectrum at high frequencies, $\nu \gg 4\gamma_{\text{max}}^2 kT_{\text{CMB}}/h$, is given by:

$$L_\nu \approx \frac{24\pi h\sigma_T}{c^2} \Gamma(p_0 - 1) \left(\frac{kT_{\text{CMB}}}{h}\right)^3 N_1 (2\gamma_{\text{max}})^{-p_0+1} \times \left(\frac{h\nu}{4\gamma_{\text{max}}^2 kT_{\text{CMB}}}\right)^{-p_0+2} \exp\left(-\frac{h\nu}{4\gamma_{\text{max}}^2 kT_{\text{CMB}}}\right) \quad (54)$$

where Γ is the gamma function. Thus, the spectrum falls off exponentially or slightly faster at high frequencies.

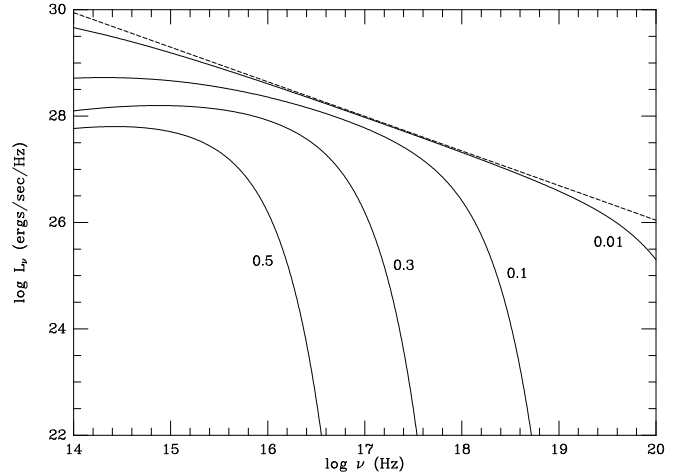


FIG. 13.— The IC emission spectra for cluster models with an initial population of electrons but no subsequent injection. The notation is similar to that in Figure 6. The solid curves show spectra for clusters which started at redshifts of $z_i = 0.01, 0.1, 0.3$, and 0.5 . These are Models 9–12 in Table 1. The dashed curve gives the spectrum for $z_i = 0$ (i.e., no evolution of the electron population due to losses).

At low frequencies, the IC spectra of these initial population only models flatten and become slowly increasing with frequency as the models age. We expect that the low energy electron spectrum in an older model with only an initial electron population will become nearly independent of γ (eq. 36 and Figure 6), except for a slowly varying logarithmic factor. If $N(\gamma) \approx N_{\text{low}}$ at low energies, where N_{low} is a constant, then the IC spectrum is given by

$$L_\nu \approx \frac{22\pi^{3/2}h\sigma_T}{5c^2} \zeta(5/2) \left(\frac{kT_{\text{CMB}}}{h}\right)^{5/2} N_{\text{low}} \nu^{1/2}, \quad (55)$$

where $\zeta(5/2) \approx 1.3415$ is the Riemann zeta function. Thus, the low frequency IC spectrum varies as $L_\nu \propto \nu^{1/2}$ for older clusters with initial electron populations only.

The spectra of models with both an initial population of particles and particle injection at the present time are shown in Figure 14. These are the models whose electron energy spectra are

given in Figure 11 (Models 23–28 and 11). The different curves represent models having differing fractions F_{inj} of the total electron energy due to the present rate of particle injection. The spectra in Figure 14 correspond to values of $F_{inj} = 100\%$, 50%, 25%, 10%, 1%, 0.1%, and 0%. Obviously, the spectrum of the models with either a pure initial electron population ($F_{inj} = 0\%$) or no initial electron population ($F_{inj} = 100\%$) are like those given in Figures 13 and 12, respectively. Models in which the current rate of particle injection provides a small but significant fraction of the total electron energy have hybrid spectra. At low frequencies ($\nu \lesssim 10^{17}$ Hz), they have an extended hump of emission, with a rapid fall off above $\nu \sim 10^{16}$ Hz. However, they also have an extended hard tail of emission at high frequencies, which has a power-law spectrum with a spectral index of $\alpha \approx -(p/2) \approx -1.15$.

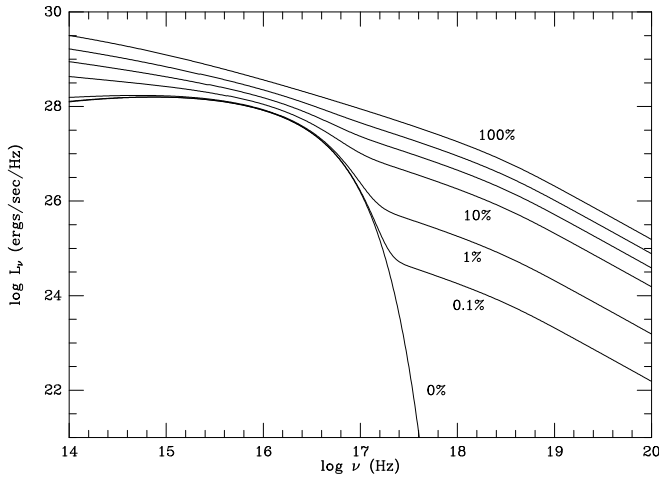


FIG. 14.— The IC emission spectra for cluster models with both an initial population of electrons (at $z_i = 0.3$) and subsequent steady injection (since $z_s = 0.05$). The models are the same as those shown in Figure 11. The values of the fraction of the particle energy which is due to the current injection are (top to bottom) $F_{inj} = 100\%$, 50%, 25%, 10%, 1%, 0.1%, and 0%. These are Models 23–28 and 11 in Table 1.

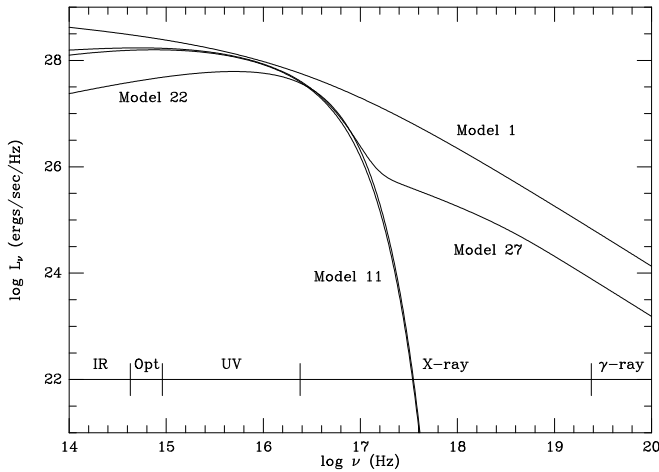


FIG. 15.— The IC emission spectra for different types of cluster models. Model 1 has continual particle injection but no initial electron population (Table 1). Model 11 has an initial electron population, but no subsequent electron injection. Model 22 is identical to Model 11, but the initial electron energy spectrum has a break at an energy of 1 GeV. Model 27 has both an initial electron population, and a source of electrons at present. The scale near the bottom of the Figure shows the portion of the electromagnetic spectrum.

The results for different types of models for the cluster electron population are summarized in Figure 15. Models 1 has continual particle injection in steady state with losses. The initial electron population in Model 11 was created at $z_i = 0.3$, but there has been no subsequent particle injection. Model 22 is identical, but the initial electron energy spectrum had a break at an energy of 1 GeV. This causes the IC spectrum to decline more rapidly toward low frequencies. Finally, Model 27 has both an initial electron population (formed at $z_i = 0.3$) and particle injection at present (since $z_i = 0.05$) which contributes 1% of the total electron population over the history of the cluster. At the bottom of Figure 15, there is a scale which shows the portion of the electromagnetic spectrum involved. The boundaries were taken to be: IR–Opt, 7000 Å; Opt–UV, 3300 Å; UV–X-ray, 0.1 keV; X-ray– γ -ray, 100 keV. We discuss several of these spectral bands separately below. Because many other processes contribute to the gamma-ray emission by these particles, I will discuss their observable gamma-ray properties in another paper. Some of the properties of the IC emission from the models for clusters are listed in Table 3. The total luminosity L_{IC} of the IC emission is given in the second column. The other entries are discussed below.

6.1. EUV and Soft X-ray Emission

Figure 15 shows that the fluxes from different models all tend to agree at frequencies $\sim 2 \times 10^{16}$ Hz, which corresponds to a photon energy of ~ 80 eV. Thus, EUV and very soft X-ray emission might be expected to be a universal property of clusters of galaxies, if they have all produced populations of relativistic electrons with total energies which are at least $\sim 10^{-2}$ of their thermal energies. The one constraint is that at least a portion of these particles must have been injected at moderate to low redshifts, $z_i \lesssim 1$. The fact that essentially all of the models produce a strong and similar flux at EUV energies may help to explain the fact the excess EUV emission has been detected in all of the cluster observed with the *Extreme Ultraviolet Explorer* (EUVE) satellite and which lie in directions of sufficiently low Galactic columns that this radiation is observable (Lieu et al. 1996a,b; Mittaz, Lieu, & Lockman 1998; Sarazin & Lieu 1998). Values of $L_\nu(\text{EUV})$ at a frequency of $\nu = 2 \times 10^{16}$ Hz are listed in column 3 of in Table 3. From these values, one finds that the emission at EUV energies is fairly directly related to $E_{CR,e}^{\text{tot}}$, the total amount of energy injected in electrons with $\gamma \geq 300$. The average relationship is about

$$L_\nu(\text{EUV}) \sim 6 \times 10^{27} \left(\frac{E_{CR,e}^{\text{tot}}}{10^{63} \text{ ergs}} \right) \text{ ergs}. \quad (56)$$

Models which are likely to apply to real clusters have spectrum which agree with equation (56) to within a factor of 4. I have also calculated the total luminosity in the EUVE observing band of photon energies of 65 to 245 eV. These values of L_{EUV} are given in column 4 of Table 3.

While the amount of EUV emission is fairly constant from model to model, the spectrum depends strongly on the amount of recent particle injection. I have fit the model spectra in the EUVE band of 65 to 245 eV to a power-law spectrum of the form $L_\nu \propto \nu^\alpha$. Specifically, $\log L_\nu$ was fit to a linear function of $\log \nu$ using the least squares method. The best-fit values of the energy spectral index α_{EUV} are listed in column 5 of Table 3. Large negative values occur for models without current particle injection and with small values of γ_{max} , where the IC

TABLE 3
INVERSE COMPTON AND RADIO EMISSION FROM MODELS

Model	L_{IC} (10^{44} ergs s^{-1})	L_{ν} (EUV) (10^{27} ergs)	L_{EUV} (10^{44} ergs s^{-1})	α_{EUV}	L_{ν} (HXR) (10^{25} ergs)	L_{HXR} (10^{44} ergs s^{-1})	α_{HXR}	L_{ν} (radio) (10^{33} ergs)	α_{radio}	L_{ν} (UV) (10^{28} ergs)	$\alpha_{Opt,UV}$
1	18.30	6.406	1.9685	-0.68	1.82	2.90	-1.12	3.41	-1.14	2.10	-0.28
2	22.86	8.002	2.4590	-0.68	2.27	3.63	-1.12	4.26	-1.14	2.63	-0.28
3	32.42	11.352	3.4884	-0.68	3.23	5.14	-1.12	6.06	-1.14	3.70	-0.28
4	44.90	15.202	4.7490	-0.64	4.52	7.20	-1.12	8.49	-1.14	4.78	-0.30
5	93.30	21.628	6.9003	-0.60	11.04	17.59	-1.12	20.75	-1.14	7.91	-0.39
6	268.00	27.269	8.5045	-0.64	44.94	74.22	-0.72	172.59	-1.08	13.63	-0.59
7	23.98	10.906	3.0394	-0.89	1.84	2.94	-1.12	3.42	-1.14	7.30	-0.54
8	8.02	4.166	1.1759	-0.86	0.58	0.92	-1.15	440.03	-1.12	1.90	-0.33
9	209.07	26.360	8.2593	-0.63	38.87	62.39	-0.85	46.61	-3.62	12.31	-0.53
10	26.44	16.356	5.2954	-0.57	0.00	0.00	—	0.00	—	4.25	-0.14
11	2.86	4.788	1.0884	-1.47	0.00	0.00	—	0.00	—	1.52	+0.00
12	0.18	0.004	0.0005	-11.93	0.00	0.00	—	0.00	—	0.41	-0.29
13	0.00	0.000	0.0000	—	0.00	0.00	—	0.00	—	0.00	—
14	11.59	14.505	3.4343	-1.33	0.00	0.00	—	0.00	—	9.25	-0.45
15	8.48	10.553	3.0849	-0.80	0.00	0.00	—	0.00	—	2.65	-0.06
16	2.89	4.828	1.1023	-1.45	0.00	0.00	—	0.00	—	1.52	+0.00
17	2.63	4.393	0.9561	-1.60	0.00	0.00	—	0.00	—	1.51	-0.01
18	1.31	1.510	0.2235	-3.31	0.00	0.00	—	0.00	—	1.37	-0.07
19	0.40	0.013	0.0016	-11.03	0.00	0.00	—	0.00	—	0.87	-0.29
20	13.18	4.826	1.4753	-0.69	1.27	2.03	-1.12	2.37	-1.14	1.58	-0.27
21	18.32	2.674	0.9804	-0.32	2.45	3.90	-1.12	4.59	-1.14	0.34	+0.10
22	2.23	4.290	1.1006	-1.16	0.00	0.00	—	0.00	—	0.54	+0.27
23	140.48	24.309	7.6864	-0.61	20.77	32.97	-1.10	39.17	-1.14	10.12	-0.46
24	71.65	14.548	4.3874	-0.71	10.39	16.48	-1.10	19.58	-1.14	5.75	-0.42
25	37.26	9.668	2.7379	-0.86	5.19	8.24	-1.10	9.79	-1.14	3.64	-0.35
26	16.62	6.740	1.7482	-1.07	2.08	3.30	-1.10	3.92	-1.14	2.37	-0.23
27	4.23	4.983	1.1544	-1.40	0.21	0.33	-1.10	0.39	-1.14	1.61	-0.04
28	3.00	4.800	1.0945	-1.46	0.02	0.030	-1.10	0.04	-1.14	1.53	-0.01

spectrum is falling off exponentially (eq. 54). Thus, a power-law may not be a good fit to the spectrum. For most of the models, the spectral index lies in the range from about -0.6 to -1.5, but very large negative values are also possible. The spectrum drops more rapidly with frequency as the proportion of electrons which are currently being injected decreases. This is most evident in Models 23-28, which are identical except for a decreasing fraction of relativistic electrons due to ongoing particle injection.

Because the *EUVE* observations of clusters have no spectral resolution, there is no detailed information on the observed spectrum of EUV emission (Lieu et al. 1996a,b; Mittaz, Lieu, & Lockman 1998). However, the ratio of *EUVE* fluxes to those in the softest bands of the *ROSAT* PSPC suggest that the EUV spectra are generally steeply declining. The spectra of the Coma cluster is less steeply declining than that of A1795; this might be understood as the result of particle acceleration by merger shocks, since Coma appears to be undergoing a merger or mergers (e.g., Burns et al. 1994; Donnelly et al. 1999), while A1795 appears regular and relaxed (e.g., Briel & Henry 1996). Also, the EUV spectra appear to get steeper with increasing radius in the A1795 cluster (Mittaz, Lieu, & Lockman 1998). This might be the result of decreasing gas density with radius; compare Models 14 and 11 in Table 3 and Figure 7.

6.2. Hard X-ray IC Emission and Radio Halos

At photon energies of 0.5 to 10 keV, the dominant emission in most clusters is the thermal emission from the hot ICM, and IC emission will be difficult to detect. However, at energies $\gtrsim 20$ keV, IC emission should again become observable, assuming that it is dropping as power-law function of frequency, while the thermal emission drops as an exponential. In Table 3, the hard

X-ray (HXR) power L_{ν} at $\nu = 10^{19}$ Hz (41.4 keV, col. 6), the luminosity L_{HXR} from 20 to 100 keV, and best-fit HXR power-law spectral index α_{HXR} from 20 to 100 keV are given for all of the models in Table 1. IC emission at photon energies of ~ 50 keV will be produced by electrons with $\gamma \sim 10^4$. These particles have rather short lifetimes ($t_{loss} \ll 10^9$ yr), and are only present in clusters in which there has been substantial particle injection since $z_i < 0.1$. As Table 3 shows, only the models with current (or very recent, as in Model 9) particle injection have any significant HXR emission.

Because of the short lifetimes of the particles producing HXR emission, these electrons are likely to be close to steady-state if present in significant quantities. The expected steady-state spectral index if IC losses dominated would be $\alpha_{HXR} = -(p+1)/2 \approx -1.65$. The best-fit spectral indices are flatter than this, $\alpha_{HXR} \approx -1.1$, mainly because other loss processes are important at the lower energy end of the HXR band (Fig. 1). With the exception of the two models in which electrons have only been injected in the cluster extremely recently (at $z_i = 0.01$, Models 6 and 9), all of the HXR spectral shapes are very similar, as expected for steady-state populations. The differences in the HXR luminosities just reflect differences in the present rate of particle injections. To a good approximation, the present day value of L_{HXR} (20–100 keV) is simply given by

$$L_{HXR} \approx 0.17 \dot{E}_{CR,e}(\gamma > 5000). \quad (57)$$

where $\dot{E}_{CR,e}(\gamma > 5000)$ is the total present rate of injection of energy in cosmic ray electrons with $\gamma > 5000$. The best-fit coefficient (0.17 in eqn. 57) depends somewhat on the power-law index of the injected electrons; the value of 0.17 applies for $p = 2.3$.

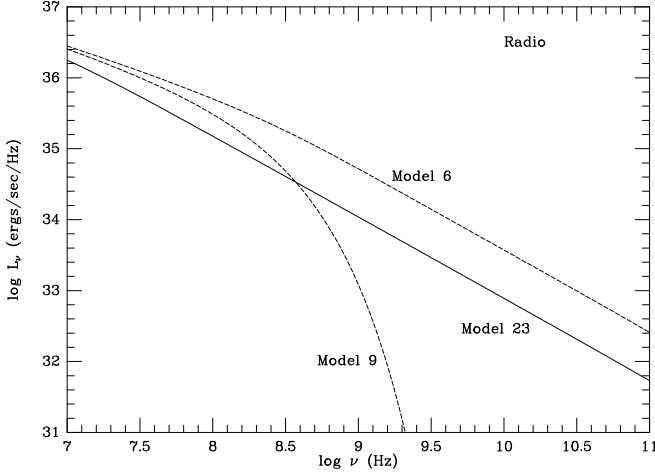


FIG. 16.— The radio synchrotron emission from three cluster models. The solid curve gives the radio spectrum of Model 23, which is typical of the models with current particle injection which has reached steady-state. Almost all of the models which have significant radio emission have spectra which are nearly identical to Model 23. In Model 6, the electrons haven't reached steady-state, and the spectrum is somewhat flatter than that of Model 23. On the other hand, in Model 9, all of the electrons were injected at $z_i = 0.01$, and the highest energy electrons have lost energy by IC and synchrotron emission. This spectrum is much steeper than Model 23 at high frequencies.

The same relativistic electrons which produce HXR emission by IC scattering will also produce radio emission by synchrotron emission. We have calculated the synchrotron radio emission from our models for the intracluster electron population. Averaging over all orientations of the magnetic field and all pitch angles for the electrons gives a radio power of

$$L_\nu = \frac{\sqrt{3}e^3 B}{m_e c^2} \int N(\gamma) R[x(\gamma)] d\gamma. \quad (58)$$

The function $R(x)$ is defined as (Ghisellini, Guilbert, & Svensson 1988)

$$R(x) \equiv 2x^2 \left\{ K_{4/3}(x) K_{1/3}(x) - \frac{3}{5} x \left[K_{4/3}^2(x) - K_{1/3}^2(x) \right] \right\}, \quad (59)$$

where K is the modified Bessel function. The normalized frequency variable x is

$$x \equiv \frac{\nu}{3\gamma^2 \nu_c}, \quad (60)$$

where ν_c is the cyclotron frequency

$$\nu_c \equiv \frac{eB}{2\pi m_e c}. \quad (61)$$

The values of the magnetic fields in the models are given in Table 1. For an electron with a given energy, the radio spectrum in equation (58) is maximum for $x \approx 0.1146$. Electrons with a Lorentz factor of γ produce radio emission with $\nu \sim 100(B/\mu G)(\gamma/10^4)^2$ MHz, and rather high electron energies ($\gamma \gtrsim 10^4$) are needed to produce observable radio emission. Thus, these are likely to be the same electrons which produce the hardest HXR emission.

Column 9 of Table 3 gives the resulting radio powers of the models at a wavelength of 91 cm ($\nu = 328$ MHz), while column 10 gives the spectral index between 91 and 21 cm ($\nu = 1.4$

GHz). The results are very similar to those for the HXR emission. Because of the short lifetimes of the high energy electrons required for radio emission, only models with very recent particle injection (at $z \lesssim 0.01$) have any significant radio emission. The high energy particles tend to be in steady state, and the radio spectra of the models tend to be quite similar. Three of the most divergent radio spectra are shown in Figure 16. The radio spectrum of Model 23 is typical of those for steady-state models with continual particle injection, and applies to most of the models with significant radio emission. In Model 6, the electrons have not yet reached steady-state, and the radio spectrum is flatter. All of the electrons in Model 9 were injected at $z_i = 0.01$, and the highest energy particles have been removed by IC and synchrotron losses. This spectrum is quite steep.

In general, HXR emission and radio synchrotron emission are expected only in clusters with very recent or current injection of relativistic electrons. Thus, both measure the current rate of particle injection. For example, if the particles are accelerated in ICM shocks, HXR and radio emission would be expected only in clusters which are currently undergoing (or which very recently underwent) a merger.

6.3. Optical and UV Emission

One also expects that the lower energy portion of the cosmic ray population in clusters will produce diffuse optical and UV emission. Diffuse optical emission is known to exist in many clusters, particularly in those with central cD galaxies (e.g., Boughn & Uson 1997). Although the origin is not completely understood, the optical colors of the diffuse light suggest that it is due to old stars, which may have been stripped from cluster galaxies. It is likely that the near or vacuum UV are better regions to detect low surface brightness diffuse emission due to IC emission, since the older stellar population in E and S0 galaxies (and, presumably, the intracluster stellar population) are fainter there.

Table 3 gives the power $L_\nu(UV)$ at a wavelength of 2000 Å and the best-fit power-law spectral index $\alpha_{Opt,UV}$ between 2000 Å and 8000 Å. The UV powers of most of the models lie within a relatively narrow range of about an order of magnitude. Unless the electron density in the ICM is much higher than 0.001 cm^{-3} and Coulomb losses are catastrophic or the electron population in clusters is very old, one would always expect a significant population of lower energy electrons. The IC spectra in the optical and UV are fairly flat, with spectral indices of $-0.5 \gtrsim \alpha_{Opt,UV} \gtrsim 0.3$. In models with current particle injection, the lower energy electron population should be approaching steady-state with the Coulomb losses (eq. 41). Then, the expected power-law for the IC emission is $\alpha \approx -(p-2)/2 \approx -0.15$. For models with only an initial electron population, the electron spectrum is expected to be nearly flat at low energies, and the spectrum is given by equation (55). Thus, the spectral index should be slightly positive in these models.

The predicted fluxes are rather low when compared to the diffuse optical emission seen in clusters of galaxies or to the sensitivity of current and UV instruments for detecting diffuse emission.

7. CONCLUSIONS

Models for the integrated population of primary cosmic ray electrons in clusters of galaxies have been calculated. The evolution of the relativistic electrons included the effects of energy losses due to IC scattering, synchrotron emission, Coulomb

losses to the ICM, and bremsstrahlung. For typical cluster parameters, the combined time scale for these losses reaches a maximum of $\sim 3 \times 10^9$ yr for electrons with a Lorentz factor $\gamma \sim 300$. This maximum loss time scale is comparable to the Hubble time or the typical age of clusters. For relativistic electrons with either much higher or lower energies, the loss time scale is considerably shorter than the typical age of a cluster.

Although the models don't depend on the detailed nature of the source of the relativistic electrons, we assume that they are accelerated by shocks, either due to the formation of the cluster and subcluster mergers, or due to radio galaxies. We present models in which the electrons are all injected at some given time in the past (e.g., the epoch of cluster formation or the time when a powerful radio galaxy is active). We also consider models with continuous electron injection, either at a constant rate or at a rate given by the self-similar solution for secondary infall onto clusters (Bertschinger 1985). Hybrid models with both initial electron populations and continual particle injection were also calculated. Based on the results for particle acceleration in supernova shocks, in most of the models we assume that the energy spectrum of the injected electrons is a power-law with an exponent of 2.3. We also consider a few models with a broken power-law, where the break occurs at the energy at which protons become relativistic.

Simple analytical solutions are given for models in which the electrons are either all injected at a single time in the past, or in which there is a constant rate of injection of electrons but no initial electron population. These solutions apply in the limits of either high or low energies, where IC and synchrotron or Coulomb losses dominate. For models in which all of the electrons were injected in the past, there is a high energy cutoff to the present electron distribution for $\gamma \geq \gamma_{\max}$. Expressions for the resulting populations and γ_{\max} were given which included synchrotron losses and the cosmological variation in IC losses due to the redshift of the CMB radiation field. At low energies where Coulomb losses dominate, the electron distribution function $N(\gamma)$ tends to a constant value, independent of γ .

Analytic solutions were also given for models with constant electron injection. At very low or high energies, the particle distribution approaches steady state. If the electrons are injected with a power-law distribution, the steady state distribution is one power steeper at high energies and one power flatter at low energies (e.g., Ginzburg & Syrovatskii 1964). A self-similar solution which connects these steady-state solutions to the time-dependent solution when the losses are not rapid was also derived.

The numerical models for the electron population are normalized such that the total energy of relativistic electrons injected with $\gamma \geq 300$ is 10^{63} ergs. For most of the models, this leads to a present-day energy in electrons with $\gamma \geq 300$ of $\sim 10^{62}$ ergs. Because the equations for the electron population are linear, models for other values can be derived by simple scaling from these values.

The most important factor affecting the energy distribution of cosmic ray electrons in the cluster models is the history of injection of the electrons. The numerical models show that only clusters in which there has been a substantial injection of relativistic electrons since $z \lesssim 1$ will have any significant population of primary cosmic ray electrons at present. For older electron populations, the high energy electrons are removed by IC losses, whose rate increases with redshift. Lower energy electrons (including initially higher energy particles which have lost energy by IC scattering) are removed by Coulomb losses.

In models with current (or very recent, $z \ll 0.1$) particle injection, the electron population is large at low energies and extends to very high energies. In models with ongoing electron injection, the distribution quickly reaches steady-state at high ($\gamma \gtrsim 300$) and low ($\gamma \lesssim 300$) energies. Due to IC losses, the high energy electron distribution is steeper than the injected one (by one exponent for a power-law injection spectrum). Coulomb losses cause the low energy distribution to be flatter than the injected spectrum (again, by one exponent for a power-law injection).

In models in which there is no current or recent particle injection, the high energy electron distribution has a cutoff for $\gamma \geq \gamma_{\max}$. Thus, no very high energy primary electrons should be present. The low energy distribution is also considerably flatter than that in models with current particle injection. In models with a large initial population of particles, but also with a significant rate of current particle injection, the electron distributions are a simple combination the behavior of the initial population models and the steady injection models. There is a steep drop in the electron population at γ_{\max} , but higher energy electrons are present at a rate determined by the current rate of particle injection. The electron population at $\gamma \lesssim \gamma_{\max}$ is fairly flat, but eventually start to increase significantly with decreasing energy at a lower energy.

Increasing (decreasing) the ICM thermal gas density decreases (increases) the number of low energy electrons ($\gamma \lesssim 100$), since these electrons are removed by Coulomb losses to the ambient plasma. If the magnetic field is greater than generally expected over most of the volume of a cluster ($B \gtrsim 3 \mu\text{G}$), synchrotron losses will reduce the number of high energy electrons beyond the effect of IC emission.

The portion of the electron spectrum where the different models exhibit the greatest level of agreement is the region near $\gamma \sim 300$, where the loss time of the electrons is maximum and where it reaches values of $\sim 3 \times 10^9$ yr, which are comparable to cluster ages. The general prediction is at all clusters should contain a significant electron population at these energies, as long as there has been significant particle injection since $z \lesssim 1$.

I also calculated the IC and synchrotron emission from these models. In models with steady particle injection with a power-law exponent p , the IC spectra relax into a steady-state form. At low energies, the spectrum is a power-law with $\alpha \approx -(p-2)/2 \approx -0.15$, while at high energies it is a power-law with $\alpha \approx -(p/2) \approx -1.15$. These two power-laws meet at a knee at $\nu \sim 3 \times 10^{16}$ Hz. In models with no current particle injection, the cutoff in the electron distribution at high energies ($\gamma \geq \gamma_{\max}$) results in a rapid drop in the IC spectrum at high frequencies. At low frequencies, the IC spectra of these models are fairly flat or even slightly rising with frequency. The IC spectra of hybrid models with both an initial population of particles and particle injection at the present time are intermediate. In models in which the current rate of particle injection provides a small but significant fraction of the total electron energy, the spectra show an extended hump at low frequencies ($\nu \lesssim 10^{17}$ Hz), with a rapid fall off above $\nu \sim 10^{16}$ Hz. However, they also have an extended hard tail of emission at high frequencies, which has a power-law spectrum with a spectral index of $\alpha \approx -(p/2) \approx -1.15$.

In the models, EUV and soft X-ray emission are nearly ubiquitous. This emission is produced by electrons with $\gamma \sim 300$, which have the longest lifetimes in clusters. The lifetimes of these particles approach the likely ages of clusters, and thus particles at this energy are likely to be present in most clus-

ters. This may explain why *EUVE* has detected EUV emission from all of the cluster observed which lie in directions of sufficiently low Galactic columns (Lieu et al. 1996a,b; Mittaz, Lieu, & Lockman 1998; Sarazin & Lieu 1998). In the models, the increase in the IC losses in going from the EUV to the soft X-ray region causes the spectral to decline rapidly in this region. More steeply declining spectra are expected in clusters without current sources of particles or with lower thermal gas densities. Assuming that the acceleration of relativistic electrons in clusters is due to ICM shocks, this may explain why the EUV spectrum in the very regular cluster A1795 is steeper than that in Coma (Mittaz, Lieu, & Lockman 1998), and why the spectrum in A1795 gets steeper at larger radii.

The IC emission also extends down in frequency into the UV, optical, and IR bands. The spectrum in this region is expected to be fairly flat, with power-law spectral indices in the range from -0.6 to $+0.3$. The steeper spectra are for models with significant current particle acceleration, while the flatter or rising spectra are for models with older electron populations and/or broken power-law electron acceleration. In the optical, the luminosities and expected surface brightnesses are below the level of diffuse stellar light observed in clusters. This emission might be easier to detect in the vacuum UV, where the older stars associated with E/S0 galaxies are fainter. However, the surface brightnesses are rather low. The UV and EUV emission from clusters might make a contribution to the diffuse extragalactic ionizing radiation, although crude estimates suggest this will not be very significant.

In much of the X-ray spectral band (from 0.5 to 10 keV), the dominant luminosity in most clusters is the thermal emission from the hot ICM, and IC emission will be difficult to detect. However, at energies $\gtrsim 20$ keV, IC emission can again become observable. I calculated the hard X-ray (HXR) IC emission from the cluster models. Radiation at these energies is produced by high energy electrons ($\gamma \sim 10^4$) which have rather short lifetimes. As a result, this emission is only expected in clusters which have current (or very recent) particle acceleration. The luminosity of HXR emission is primarily determined by the current rate of particle acceleration in the cluster. The same particles which produce HXR radiation by IC scattering will also produce radio emission by synchrotron emission at

observable frequencies. I have also calculated the radio spectra produced by the models. In general, the high energy electrons which produce the HXR and radio emission should be nearly in steady-state, and the predicted spectra for most models with significant HXR or radio emission are approximately power-laws with spectral indices of $\alpha \approx -1.1$.

If the main source of primary relativistic electrons is acceleration in ICM shocks, then HXR tails and diffuse radio halos should be confined to clusters which currently have strong ICM shocks. Thus, we would expect that these would mainly be clusters presently undergoing significant mergers. In the case of radio halos, there is some evidence that this is indeed the case (e.g., Tribble 1993). At the same time, large cluster radio halos are quite rare. This may be related to the short lifetimes of the high energy particles required and to the need for the merger to be at a stage where the shocks are very strong; alternatively, some other physical properties (e.g., magnetic field intensity or geometry, or high shock Mach number, ...) may be required to produce high energy electrons in ICM shocks.

Because the HXR and radio halo emissions are produced by particles with very short lifetimes while the EUV emission is due to electrons whose lifetimes are a significant fraction of the likely ages of clusters, one would not expect the same power-law spectrum which fits the HXR and radio emission to extend to the EUV emission. In fact, EUV emission is seen from clusters with no detectable radio halo emission (such as A1795), so it is clear that the EUV and HXR/radio cannot be connected with a single power-law spectrum with a normal spectral index. The EUV and HXR/radio should connect continuously in clusters where a large fraction of the cosmic ray electrons are being generated at the present time (i.e., in an ongoing or very recent strong merger). In the more general case, one expects a broad peak in the IC emission in the EUV band, a rapid drop-off in the spectrum from the EUV to the X-ray band, and HXR/radio emission proportional to the present rate of particle acceleration (Figures 14 and 15).

This work was supported in part by NASA Astrophysical Theory Program grant NAG 5-3057. I thank Richard Lieu and Andy Fabian for helpful conversations or correspondence.

REFERENCES

- Bell, A. R. 1978a, *MNRAS*, 182, 147
 Bell, A. R. 1978b, *MNRAS*, 182, 443
 Berezhinsky, V. S., Blasi, P., & Ptuskin, V. S. 1997, *ApJ*, 487, 529
 Bertschinger, E. 1985, *ApJS*, 58, 39
 Blandford, R. D., & Eichler, D. 1987, *Phys. Rep.*, 154, 1
 Blandford, R. D., & Ostriker, J. P. 1978, *ApJ*, 221, L29
 Blumenthal, G. R., & Gould, R. J. 1970, *RMP*, 42, 237
 Boughn, S. P., & Uson, J. M. 1997, *ApJ*, 488, 44
 Briel, U. G., & Henry, J. P. 1996, *ApJ*, 472, 131
 Burns, J. O., Roettiger, K., Ledlow, M., & Klypin, A. 1994, *ApJ*, 427, 87
 Cavaliere, A., Gursky, H., & Tucker, W. H. 1971, *Nature*, 231, 437
 Colafrancesco, S., & Blasi, P. 1998, preprint (astro-ph/9804262)
 Deiss, B. M., Reich, W., Lesch, H., & Wielebinski, R. 1997, *A&A*, 321, 55
 Donnelly, R. H., Markevitch, M., Forman, W., Jones, C., Churazov, E., & Gilfanov, M. 1999, *ApJ*, in press
 Enßlin, T. A., & Biermann, P. L. 1998, *A&A*, 330, 90
 Fusco-Femiano, R., Dal Fiume, D., Feretti, L., Giovannini, G., Matt, G., & Molendi, S. 1998, preprint (astro-ph/9808012)
 Ghisellini, G., Guilbert, P. W., & Svensson, R. 1998, *ApJ*, 334, L5
 Ginzburg, V. L., & Syrovatskii, S. I. 1964, *The Origin of Cosmic Rays* (New York: MacMillan)
 Giovannini, G., Feretti, L., Venturi, T., Kim, K. T., & Kronberg, P. P. 1993, *ApJ*, 406, 399
 Goldoni, P., et al., 1998, preprint
 Hanisch, R. J. 1982, *A&A*, 111, 97
 Henriksen, M. J. 1988, preprint (astro-ph/9807049)
 Hwang, C.-Y. 1997, *Science*, 278, 1917
 Jones, F. C., & Ellison, D. C. 1991, *SSRv*, 58, 259
 Kaastra, J. S., Bleeker, J. A. M., & Mewe, R. 1998, preprint
 Kim, K.-T., Kronberg, P. E., Dewdney, T. L., & Landecker, T. L. 1990, *ApJ*, 355, 29
 Kim, K.-T., Kronberg, P. E., & Tribble, P. C. 1991, *ApJ*, 379, 80
 Kronberg, P. E. 1994, *Rep. Prog. Phys.*, 57, 1994
 Lieu, R., Mittaz, J. P. D., Bowyer, S., Breen, J. O., Murphy, E. M., Lockman, F. J., & Hwang, C.-Y. 1996a, *Science*, 274, 1335
 Lieu, R., Mittaz, J. P. D., Bowyer, S., Lockman, F. J., Hwang, C.-Y., & Schmitt, J. H. M. M. 1996b, *ApJ*, 458, L5
 Mittaz, J. P. D., Lieu, R., & Lockman, F. J. 1998, *ApJ*, 498, L17
 Press, W. H., Flannery, B. P., Teukolsky, W. A., & Vetterling, W. T. 1986, *Numerical Recipes: The Art of Scientific Computing*, (Cambridge: CUP), 563–568
 Rephaeli, Y. 1979, *ApJ*, 227, 364
 Rephaeli, Y., Ulmer, M., & Gruber D. 1994, *ApJ*, 429, 554
 Sarazin, C. L. 1988, *X-ray Emission from Clusters of Galaxies* (Cambridge: Cambridge Univ. Press)
 Sarazin, C. L., & Lieu, R. 1998, *ApJ*, 494, L177
 Tribble, P. C. 1993, *MNRAS*, 263, 31
 Weinberg, S. 1972, *Gravitation and Cosmology: Principles and Applications of the General Theory of Relativity* (New York: Wiley), 481–484
 Wilson, M. A. 1970, *MNRAS*, 151, 1